Mechanism of Auxiliary Subunit Modulation of Neuronal α_{1E} Calcium Channels

Lisa P. Jones, Shao-kui Wei, and David T. Yue

From the Program in Molecular and Cellular Systems Physiology, Departments of Biomedical Engineering and Neuroscience, Johns Hopkins University School of Medicine, Baltimore, Maryland 21205

ABSTRACT Voltage-gated calcium channels are composed of a main pore-forming α_1 moiety, and one or more auxiliary subunits (β, $\alpha_2\delta$) that modulate channel properties. Because modulatory properties may vary greatly with different channels, expression systems, and protocols, it is advantageous to study subunit regulation with a uniform experimental strategy. Here, in HEK 293 cells, we examine the expression and activation gating of α_{1E} calcium channels in combination with a β (β_1–β_4) and/or the $\alpha_2\delta$ subunit, exploiting both ionic- and gating-current measurements. Furthermore, to explore whether more than one auxiliary subunit can concomitantly specify gating properties, we investigate the effects of cotransfecting $\alpha_2\delta$ with β subunits, of transfecting two different β subunits simultaneously, and of COOH-terminal truncation of α_{1E} to remove a second β binding site. The main results are as follows. (*a*) The $\alpha_2\delta$ and β subunits modulate α_{1E} in fundamentally different ways. The sole effect of $\alpha_2\delta$ is to increase current density by elevating channel density. By contrast, though β subunits also increase functional channel number, they also enhance maximum open probability (G_{max}/Q_{max}) and hyperpolarize the voltage dependence of ionic-current activation and gating-charge movement, all without discernible effect on activation kinetics. Different β isoforms produce nearly indistinguishable effects on activation. However, β subunits produced clear, isoform-specific effects on inactivation properties. (*b*) All the β subunit effects can be explained by a gating model in which subunits act only on weakly voltage-dependent steps near the open state. (*c*) We find no clear evidence for simultaneous modulation by two different β subunits. (*d*) The modulatory features found here for α_{1E} do not generalize uniformly to other α_1 channel types, as α_{1C} activation gating shows marked β isoform dependence that is absent for α_{1E}. Together, these results help to establish a more comprehensive picture of auxiliary-subunit regulation of α_{1E} calcium channels.

KEY WORDS: calcium channels • α_{1E} • gating currents • subunit modulation • heterologous expression

INTRODUCTION

Voltage-gated calcium channels are molecular transducers that trigger cellular processes ranging from muscle contraction to neurotransmission. Modulation of these channels thereby constitutes a key potential mechanism for functional adaptation and plasticity. At least three different subunits are believed to comprise native calcium channels: a main, pore-forming α_1 subunit, a cytoplasmic β subunit, and a disulfide-linked $\alpha_2\delta$ subunit (for review, see Perez-Reyes and Schneider, 1994; De Waard et al., 1996). So far, seven different genes encoding $\alpha_{1A,B,C,D,E,S,G}$ subunits, and four different genes encoding $\beta_{1,2,3,4}$ subunits have been identified, along with multiple splice variants. Given this heteroligomeric structure, regulation of channel properties by variations in subunit composition have been widely studied as a potential mechanism for tuning channel gating properties to support a given physiologic role.

Address correspondence to David T. Yue, Program in Molecular and Cellular Systems Physiology, Departments of Biomedical Engineering and Neuroscience, Johns Hopkins University School of Medicine, Ross Building, Room 713, 720 Rutland Avenue, Baltimore, MD 21205. Fax: 410-955-0549; E-mail: dyue@bme.jhu.edu

Despite the potential importance of modulation by subunit combination, fundamental uncertainties remain about the effects of auxiliary subunits (for review see Perez-Reyes and Schneider, 1994; De Waard et al., 1996; Walker and De Waard, 1998). While coexpression studies have demonstrated that the addition of auxiliary subunits (β, $\alpha_2\delta$) can have striking effects on channel gating and/or channel expression, the specific effects observed vary across studies, even using the same α_1 subunit. At least some of the differences in subunit effects may reflect isoform-specific variations in the effects of distinct β subunit isoforms on α_1 gating. Further variability may arise from the use of diverse expression systems, electrophysiological methods, and experimental solutions. These points underscore the need to explore subunit modulation of each α_1 isoform individually, and to undertake comprehensive studies with uniform experimental conditions.

Although most previous work has focused on α_{1C}, neuronal α_{1E} channels (Soong et al., 1993) have recently emerged as important channels with which to attempt such comprehensive investigation for several reasons. First, subunit modulation of α_{1E} has potential physiological relevance, as α_{1E} (presumed "R-type") channels have

been implicated in neuronal functions including neurotransmitter release (Wu et al., 1998). Second, α_{1E} demonstrates an exceptional capacity for high-level recombinant expression, which permits well-resolved measurements of both ionic and gating currents, even when the α_{1E} subunit is expressed alone (which generally lowers overall expression of current). This capability enables examination of changes in both peak open probability and channel density (Olcese et al., 1996), two critical measures for resolving how auxiliary subunits affect the overall level of calcium current. Third, β subunits may affect α_{1E} expression in a uniquely different manner than observed with other pore-forming α_1 subunits, providing a potentially useful clue as to the underlying mechanism of subunit modulation. Olcese et al. (1994, 1996) provide the most biophysically detailed results in this regard, using *Xenopus* oocytes. In contrast to other α_1 subunits, β subunits caused little change or even a decrease in overall α_{1E} current density. This outcome resulted from decreased channel density, as assessed by maximal gating charge, countered by increased channel opening. By contrast, in mammalian expression systems, β subunits increased overall α_{1E} current density (Williams et al., 1994; Stephens et al., 1997). Here, however, no α_{1E} gating-current measurements have been made to permit assessment of underlying changes in channel density and open probability. Finally, α_{1E} is one of the channels in which a second β binding site has been explicitly identified (Tarelius et al., 1997; Walker et al., 1998). Characterization of mutant α_{1E} constructs lacking this site would allow determination of the functional importance of the secondary site.

Here, we therefore examine subunit modulation of α_{1E} channels coexpressed with various combinations of auxiliary subunits (β_1–β_4, $\alpha_2\delta$) in mammalian HEK 293 cells. The same recombinant expression system, along with a consistent set of experimental solutions and protocols, is used throughout to facilitate direct comparison of channels with differing molecular composition. Measurements of both ionic and gating currents permits in-depth analysis of subunit modulatory effects. We focus on three key questions. (*a*) To what degree does modulation of α_{1E} current density reflect modulation of channel gating and/or number of functional channels? (*b*) How do different auxiliary subunits compare with regard to modulation of activation gating? (*c*) What is the functional impact of the secondary β binding site in α_{1E}? Through addressing these questions, this study helps to establish a more refined picture of auxiliary-subunit modulation of α_{1E} calcium channels.

MATERIALS AND METHODS

Expression of N-Type Channels

HEK 293 cells, obtained from Dr. Jeremy Nathans (Johns Hopkins University; Gorman et al., 1990), were grown at 37°C in Dulbecco's modified Eagles medium (GIBCO BRL, Grand Island, NY), 10% fetal calf serum (GIBCO BRL), 1% L-glutamine (Sigma Chemical Co., St. Louis, MO), 1% penicillin-streptomycin (P0906; Sigma Chemical Co.), in 5% CO_2. Low-passage number cells were used (<P20). cDNAs encoding channel subunits α_{1E} (Soong et al., 1993), α_{1C} (Wei et al., 1991), β_{1b} (Pragnell et al., 1991), β_{2a} (Perez-Reyes et al., 1992), β_3 (Castellano et al., 1993*b*), β_4 (Castellano et al., 1993*a*), and $\alpha_2\delta$ (Tomlinson et al., 1993) were subcloned into mammalian expression plasmids (pMT2; Genetics Institute, Cambridge, MA, for β_4, pZEM229R; ZymoGenetics, Inc., Seattle, WA, for $\alpha_2\delta$, pGW1; British Biotechnologies, Cowley, Oxford, UK for all others). $\alpha_{1E\Delta}$ was constructed by replacing the Bst 1107I (α_{1E}: nucleotide 4299, given start codon at nucleotide 1) and SalI (3′ polylinker) region of α_{1E} in pGW1 with a shorter polymerase chain reaction fragment, including a premature stop codon after the codon for amino acid 1871. The portion of the channel derived from PCR was verified in its entirety with the use of the fluorescent dideoxy terminator method of thermocycle sequencing on an automated DNA sequencer (Applied Biosystems Division 373a; Perkin-Elmer Cetus Instruments, Emeryville, CA). HEK 293 cells were transiently transfected using a standard, calcium-phosphate precipitation procedure (Brody et al., 1997) with a total of 30 μg of DNA per 10-cm plate. 10 μg of a plasmid containing a pore forming subunit was included (α_{1E} or α_{1C}) and mixed with 10 μg of each desired auxiliary subunit (none, a β subunit, and/or the $\alpha_2\delta$ subunit). If the amount of DNA totaled <30 μg, pBluescript was added to make up the difference. For certain experiments, both β_{2a} and β_3 were simultaneously transfected either in a 1:1 ratio (10 μg of each plasmid) or a 5:1 ratio (15 μg of β_3, 3 μg of β_{2a}). More than 20% of cells transfected with a pore forming subunit exhibited detectable high-threshold calcium currents.

"Mock-transfected" cells were transfected with 10 μg of β_{1b}, 10 μg of $\alpha_2\delta$, and 10 μg of pBluescript. In our usual ionic current recording conditions (detailed below), we observed no high threshold, voltage-gated, calcium-channel currents in such cells ($n = 32$ cells, over two independent rounds of transfection), or in cells transfected with the β_{2a} subunit alone ($n > 40$ cells; Patil et al., 1998). In mock-transfected cells, we occasionally (~10% of cells) observed endogenous, low threshold calcium channel currents of small amplitude (peak ionic current ~20 pA in 10 mM Ba^{2+}), as reported previously by Sun et al. (1994). Although endogenous currents of such small amplitude would contribute negligibly to our results, cells with low threshold activity were nevertheless rejected. At the biochemical level, Western blots performed on total membrane protein (30 μg/lane) from untransfected cells revealed no known high threshold α_1 (A, B, C, D, E) or β (1b, 2e, 3a, 4) subunits, and only low levels of $\alpha_2\delta$ (personal communication, Mark Williams, SIBIA Neurosciences Inc., La Jolla, CA). Blots were probed individually with appropriate antibodies, and the lack of subunit proteins was gauged from the absence of bands that were clearly present using cells transfected with corresponding recombinant subunits. The result that coexpression of $\alpha_2\delta$ with α_{1E} potentiated current by approximately threefold suggests that trace expression of endogenous $\alpha_2\delta$ did not significantly influence our results.

Electrophysiology

Whole-cell recordings were obtained at room temperature 48–72 h after transfection using an Axopatch 200A (Axon Instruments, Foster City, CA) and standard patch-clamp techniques. Cell capacitance ranged from 10–40 pF. Series resistance was typically <5 MΩ, and compensated 70–85%, resulting in a typical settling time of ~80 μs. Voltage pulses were delivered every 15–20 s from a holding potential of −110 mV, except for prepulse inactivation

protocols, where voltage pulses were given every minute from a holding potential of −120 mV to allow recovery from inactivation. Data were typically acquired at 50 kHz and filtered at 10 kHz (−3 dB, four-pole Bessel). Displayed traces have generally been additionally processed with a gaussian digital filter at 2 kHz. Leak and capacity currents were subtracted by a P/8 protocol (ionic currents) or P/−8 protocol (gating currents) from the −110-mV holding potential, unless otherwise noted (Armstrong and Bezanilla, 1974). To allow better resolution of small currents, we often subtracted a smooth curve fitted to the leak currents. In some cases, the first 200 μs after a voltage step contains a large leak subtraction artifact, which was zeroed when present before digital filtering.

The base external solution contained (mM) 155 *N*-methyl-D-glucamine (NMG) aspartate, 10 HEPES, 10 4-aminopyridine, 0.1 EGTA, pH 7.4 with NMG, 280–300 mOsm with no added charge carriers. The internal solution contained (mM) 150 NMG-methanesulfonate ($MeSO_3$), 1 $MgCl_2$, 4 MgATP, 10 HEPES, 10 EGTA, pH 7.3, with NMG, typically 280–290 mOsm. The h(∞)-V relations shown in Fig. 11 for α_{1C} were obtained with an internal solution in which the 150 mM NMG-$MeSO_3$ was replaced by 150 mM Cesium-$MeSO_3$. For measurement of ionic currents, either 2 or 10 mM $BaCl_2$ was added to the external solution. For typical gating current measurements, 0.2 mM $LaCl_2$/2 mM $MgCl_2$ was added. External solution flowed continuously at a rate of 1–2 ml/min during recording. The bath solution was grounded by a 0.5 M KCl agar bridge attached to a Ag-AgCl wire. Measurements were started after >5 min of dialysis with the internal solution. In all cases, the junction potential between external and internal solutions was ~5 mV (Neher, 1992). To determine the true applied potential, this value should be added to the voltages in the figures and text.

For measurement of α_{1E} activation curves, 2 mM $BaCl_2$ was the charge carrier throughout. Test depolarizations were 30 ms long and ranged from −70 to +70 mV (see Fig. 2 *A, top*) with repolarization to −50 mV to allow good resolution of tail currents. For each cell, plots of peak tail current at −50 mV (I_{tail}) vs. test pulse voltage (V_{test}) were normalized by an estimate of maximal peak tail current ($I_{tail,max}$). $I_{tail,max}$ was taken as the saturating value of Boltzmann fits to the I_{tail}-V_{test} data. The resulting normalized relations are equivalent to normalized P_o-V relations, and are referred to as G-V curves. G-V curves were then averaged across cells. Such G-V curves were indistinguishable from G-V relations obtained using 15-ms test depolarizations (data not shown). We did not correct tail currents for the contribution of the "OFF" gating current. To assay the magnitude of the error that such OFF gating currents might produce, we corrected G-V relations for six cells transfected with $\alpha_{1E}\beta_{2a}$ by subtracting the OFF gating currents measured during repolarization to −50 mV. We found that the average single-Boltzmann fit parameters for the corrected and uncorrected G-V curves were statistically indistinguishable ($P < 0.05$, Student's *t* test, uncorrected: $z = 3.51 \pm 0.4$, $V_{1/2} = -20.1 \pm 3.2$ mV; corrected: $z = 3.57 \pm 0.5$, $V_{1/2} = 19.7 \pm 3.4$ mV), although $I_{tail,max}$ was reduced by ~5% (−2,638 ± 568 pA [uncorrected] vs. 2,516 ± 542 pA [corrected]). G_{max} was calculated according to $G_{max} = I_{tail,max}/(V - V_{rev})$, where V_{rev} was +40 mV in 2 mM $BaCl_2$. Therefore, the small error in $I_{tail,max}$ will lead to a slight overestimate of the G_{max}/Q_{max} ratio, which may vary slightly for the different subunit combinations.

For gating currents, ionic currents were blocked by the external solution containing 0.2 mM $LaCl_3$ (Bean and Rios, 1989). The effective free La^{3+} concentration was 0.1 mM due to the presence of 0.1 mM EGTA in all external solutions. The voltage protocol was the same as for ionic currents, except that the test pulse duration was decreased to 15 ms, and repolarization to −110 mV (see Fig. 5 *A, top*). Total charge moved during test depolarization (Q_{on}) was obtained by integrating over the entire depolarizing epoch, taking as the zero baseline the average current over the last 3 ms of the test pulse. Total charge moved during repolarization (Q_{off}) was calculated similarly. For each cell, Q_{on}-V and Q_{off}-V curves were normalized by an estimate of maximal mobile charge (Q_{max}), taken as the saturating value of the Boltzmann fit (detailed below) to the Q_{on}-V or Q_{off}-V curves, as indicated in the text. Such normalized Q_{on}-V and Q_{off}-V curves were averaged across cells.

To ensure that La^{3+} does not alter activation gating, we obtained Q-V relations both in the presence and absence of La^{3+} blockade. Fig. 1 *A* shows the results of the analysis, in which we compared Q_{off}-V curves acquired in 2 mM $MgCl_2$ (●) and 2 mM $MgCl_2$/0.2 mM $LaCl_3$ (○). The identity of the two curves, absent the expected surface-potential shift, provides additional strong support that La^{3+} does not perturb activation gating.

To determine explicitly the surface-charge shift between solutions used for ionic and gating currents, we exploited the property that isolated gating currents can actually be measured in the solution for ionic current, so long as the voltage range is negative to the threshold (~−65 mV, Fig. 1 *B, inset*) for ionic-current activation. We could then calculate the surface-charge shift by direct comparison of the rising "foot" of Q-V curves obtained in ionic and gating current solutions. Fig. 1 *B* shows the results of this approach. Before averaging across cells, Q-V data for a single cell was normalized by the value of Q_{on} at −65 mV in 2 mM Ba^{2+}. In the ionic-current solution containing 2 mM Ba^{2+}, the Q_{on}-V (Fig. 1 *B, inset,* ○) and Q_{off}-V (*inset,* ●) curves matched at potentials negative to −65 mV, indicating that gating currents were isolated below this potential. The main graph in Fig. 1 *B* demonstrates that, over this range of voltages, Q_{on}-V relations obtained in 2 mM Ba^{2+} (○) and 2 mM $MgCl_2$/0.2 $LaCl_3$ (◇) are essentially indistinguishable, indicating that there is little if any surface-charge shift between solutions. To quantitate the value of the shift, for each cell the voltage shift required to fit the same dual-Boltzmann to both sets of Q_{on}-V data was taken to be the surface potential difference. Averaging this value across cells gave a value of 3 ± 1 mV ($n = 9$). These results excluded the need for surface-charge correction between ionic and gating current measurements.

Steady state inactivation curves were approximated using a protocol in which a 20-s prepulse was followed by a step to peak of the current–voltage (I-V)[1] curve (typically −5 mV) to measure the fraction of inactivated current. In some cases, a 10-ms normalizing prepulse at the test pulse potential was included before the 20-s prepulse to assay for the presence of cumulative inactivation or rundown. Steady state inactivation (h(∞)-V) curves were derived by normalizing test pulse currents by either the current during the normalizing test pulse, or by the value of the test pulse with no prepulse. All steady state inactivation curves were measured with 10 mM Ba^{2+} as charge carrier. Voltage commands were given every minute from a holding potential of −120 mV. Typically, prepulse voltages ranged from −120 to −20 mV in 10-mV increments. Normalized h(∞)-V relations were averaged across cells. For cells transfected with two β subunits, the h(∞)-V relation was fit with a dual-Boltzmann function to obtain parameters for the low and high threshold components, in addition to the relative contribution of each component.

Boltzmann fits to either G-V or Q-V relations were performed with functions of the form $B(V) = B_{max}/\{1 + \exp[-zF(V - V_{1/2})/RT]\}$, where B_{max} is the saturating value, *z* is the effective charge, and $V_{1/2}$ is the midpoint of activation. Q_{on}-V data above +40 mV were sometimes unreliable and were therefore excluded.

[1]*Abbreviation used in this paper:* I-V, current–voltage.

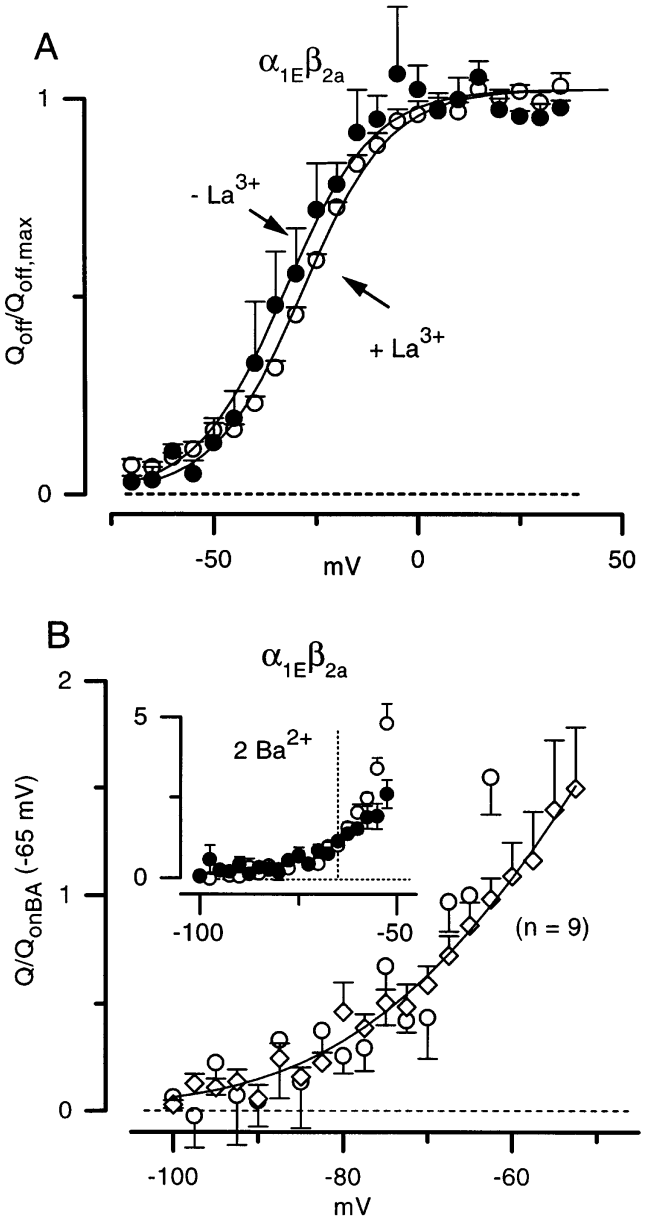

FIGURE 1. La^{3+} control experiments. (*A*) La^{3+} does not change the voltage dependence of charge movement. Comparison of average Q-V relations in 2 mM Mg^{2+} (●, $n = 6$) and 2 mM Mg^{2+}/0.2 mM La^{3+} (○, same cells). Solid lines represent Boltzmann fits to the data without ($V_{1/2} = 32.8$ mV, $z = 2.4$) and with ($V_{1/2} = 28.5$ mV, $z = 2.4$) La^{3+}. (*B*) Estimate of surface charge shift between 2 mM Ba^{2+} and 2 mM Mg^{2+}/0.2 mM La^{3+}. (*main plot*) Comparison of averaged Q_{on}-V relations ($n = 9$) measured in 2 mM Ba^{2+} (○) and 2 mM Mg^{2+}/0.2 mM La^{3+} (◇) to demonstrate the absence of an appreciable surface charge shift. Solid line is a dual-Boltzmann fit by eye to the 2 mM Mg^{2+}/0.2 mM La^{3+}data. (*inset*) Plot of averaged Q_{on}-V (○) and Q_{off}-V (●) relations measured in 2 mM Ba^{2+} to illustrate the threshold of activation (~65 mV, *dotted vertical line*). For voltages past the threshold of activation, the presence of ionic current shifts the baseline used in the calculating Q_{on}; as a result, Q_{on} is overestimated and appears larger than Q_{off} for these voltages.

For dual-Boltzmann fits to h(∞)-V relations, we used a function of the form $B(V) = f_{low}\{1 + \exp[z_{low} F(V - V_{1/2,low})/RT]\}^{-1} + f_{high}\{1 + \exp[z_{high} F(V - V_{1/2,high})/RT]\}^{-1}$, where $V_{1/2,low}$ and $V_{1/2,high}$ are midpoints of activation, z_{low} and z_{high} are the effective valences, and f_{low} and f_{high} are amplitudes of low and high threshold components. Fits were obtained using nonlinear, least-squares minimization. All reported values are mean ± SEM.

RESULTS

Enhancement of Expressed Current Density by Auxiliary Subunits

Transfection of HEK 293 cells with the α_{1E} subunit alone, or in combination with various auxiliary subunits, led to the expression of well-resolved inward barium currents carried by recombinant calcium channels (Fig. 2 *A*). The relative magnitudes of the various sets of traces illustrate that addition of auxiliary subunits caused striking increases in the level of expressed current. To quantify the relative increase in current density, we calculated the maximum tail current upon repolarization to 50 mV [$G_{max} = nP_{o,max}\, g(-50\text{ mV})\, h$], where g is the unitary conductance, h is the fraction of noninactivated channels at the end of the test pulse, n is the number of channels, and $P_{o,max}$ is the maximum open probability. Fig. 2 *B* compares the average values of G_{max} for all different subunit combinations examined. The largest effect was the ~12-fold enhancement of expressed current with the coexpression of β subunits. All β subunits were approximately equipotent in this regard, although the average β_3 effect was slightly smaller (approximately sevenfold). Addition of $\alpha_2\delta$ to α_{1E} produced a weaker increase in current (about threefold), and the combination of $\alpha_2\delta$ and β subunits yielded no appreciable current enhancement over the coexpression of β subunits alone. Since modulation of G_{max} values may reflect not only changes in $nP_{o,max}$, but also differences in the number of noninactivated channels (h) with different subunits, we examined another measure of current density (Fig. 2 *C*), $I_{peak} = nP_o[V_{peak}]\, i[V_{peak}]$, where $P_o[V_{peak}]$ and $i[V_{peak}]$ are the open probability and unitary current at the voltage (V_{peak}) yielding the maximum test-pulse current. This measure (I_{peak}), which is less sensitive to test pulse inactivation, gave similar results. Therefore, we are confident that G_{max} can henceforth be used as a quantitative indicator of relative changes in current ($nP_{o,max}$).

Isolation of Gating Currents from Channels Containing the α_{1E} Subunit

To determine the origin of the increased current density ($nP_{o,max}$), we wished to measure the maximum amount of mobile gating charge ($Q_{max} = nq$, q is the charge per channel), which provides a convenient assay for the relative number of functional channels (n). Measuring Q_{max} involves good resolution of the cur-

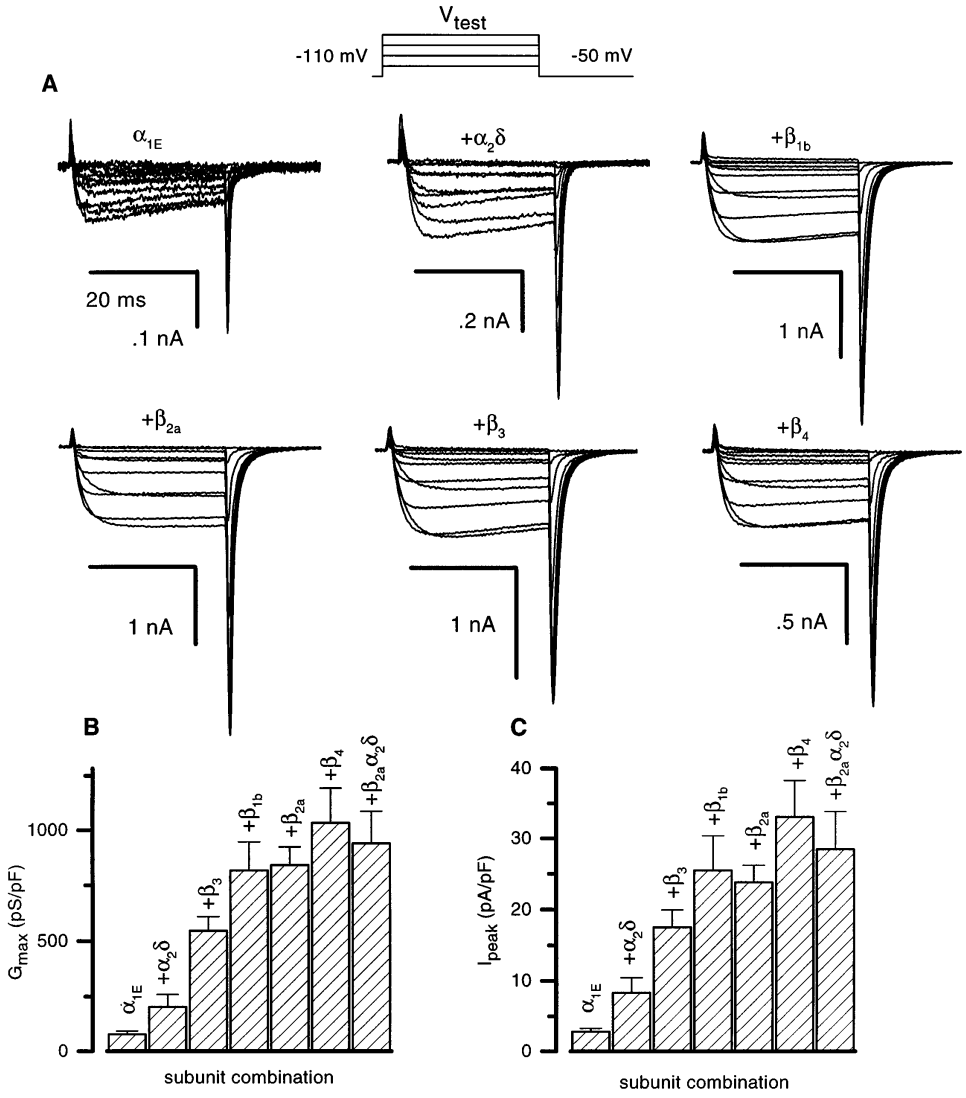

FIGURE 2. Modulation of ionic current density by β subunits. (*A*) Ionic currents in response to the protocol (*top*) used to measure the voltage dependence of ionic activation. Currents were measured with 2 mM Ba^{2+} as charge carrier in response to voltage steps ranging from −50 to 50 mV in 10-mV increments for the indicated subunit combinations. (Cells 93_16 [α_{1E}], 174_3 [$+\alpha_2\delta$], 296_4 [$+\beta_{1b}$], 252_5 [$+\beta_{2a}$], 306_21 [β_3], and 296_25 [β_4].) (*B* and *C*) Comparison of the effects of auxiliary subunits on expressed current density, assayed by normalizing either the maximal conductance (G_{max}) derived from the peak tail current (*B*) or the peak current I_{max} (*C*) by the cell capacitance. Values are listed in Table I.

rents arising from gating charge movement (gating currents; Armstrong and Bezanilla 1977; Sigworth, 1994), which in turn requires a blocker that eliminates ionic currents without significantly perturbing channel gating behavior. Previous work indicates that the highly potent block by La^{3+} can be used to isolate gating currents of calcium channels containing the α_{1B} subunit (Jones et al., 1997*a*), but not the α_{1C} subunit (Kamp et al., 1996). To determine the feasibility of La^{3+} blockade of calcium channels containing α_{1E}, we examined gating currents with either 2 mM Ba^{2+} or 2 mM Mg^{2+}/0.2 mM La^{3+} added to the bath solution (Fig. 3 *A*). Although 2 mM Mg^{2+}/0.2 mM La^{3+} (*solid traces*) completely blocked ionic currents, the early outward transients that are dominated by gating current were unchanged, arguing strongly that La^{3+} does not alter the voltage sensor movement that underlies activation gating. Furthermore, the block of ionic current was completely reversible (Fig. 3 *B*, ●), and did not alter Q_{rev} during repetitive stimulation in the presence of La^{3+} (○, obtained by integrating outward transients at the reversal potential). The lack of change of Q_{rev} argues that La^{3+} does not promote channel inactivation, which would be apparent as a reduction in Q_{rev} (Jones et al., 1997*b*) known as gating-charge immobilization (Armstrong and Bezanilla, 1977; Bezanilla et al., 1991). Similar results to those for α_{1E} + β_{2a} (Fig. 3, *A* and *B*) were obtained with the other subunit combinations (data not shown). Further experiments (see MATERIALS AND METHODS) demonstrated that La^{3+} did not affect the voltage dependence of charge movement, and that the surface charge shift between solutions used for ionic and gating current measurements was ~3 mV.

With assurance that La^{3+} does not detectably alter gating or surface-charge properties, we turned to analysis of extensive sets of currents recorded during La^{3+}

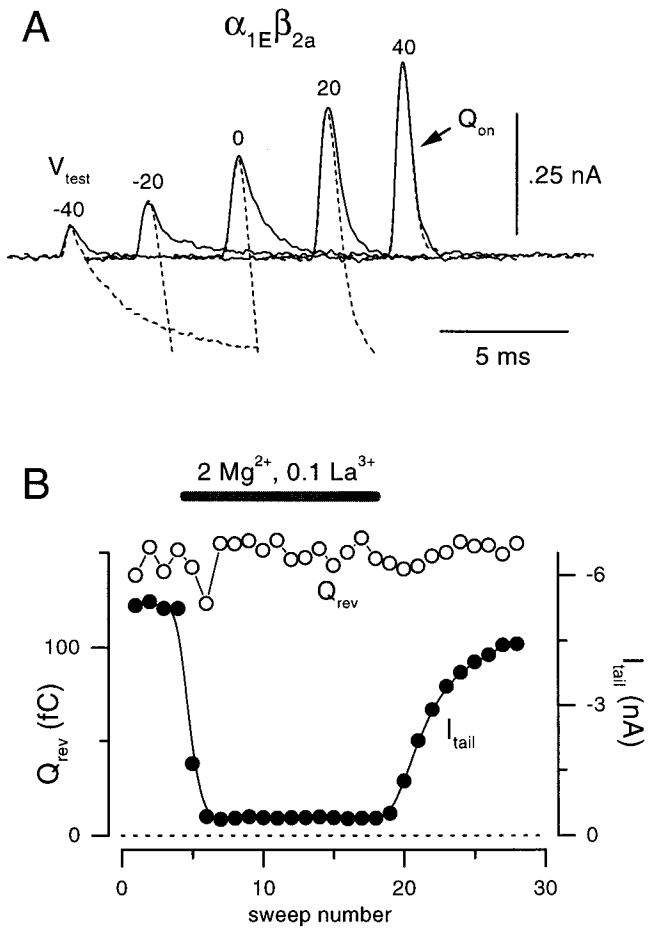

FIGURE 3. Control experiments on $\alpha_{1E}\beta_{2a}$-transfected cells to assay the effect of La^{3+} block on channel gating. (*A*) Whole-cell currents elicited by 15-ms test depolarizations from a holding potential of −110 mV. For each test potential, the currents measured with either 2 mM Ba^{2+} (*dashed line*) or 2 mM Mg^{2+}/0.2 mM La^{3+} (*solid line*) in the external solution are superimposed to demonstrate that ionic current blockade by La^{3+} does not alter the gating-charge movement. Cell 320_6. (*B*) Diary plot recorded from an $\alpha_{1E}\beta_{2a}$-transfected cell in response to 15-ms depolarizations to the reversal (~40 mV) every 15 s. Q_{rev} was derived by integrating the "ON" gating current transient; I_{tail} was measured as the peak tail current upon repolarization to −50 mV. Bar indicates the application of the 2 mM Mg^{2+}/0.2 mM La^{3+} block solution. Cell 292_12.

block for $\alpha_{1E}\beta_{2a}$ (Fig. 4 *A*). These traces represent genuine calcium-channel gating currents for several reasons. First, no such currents are observed in mock-transfected cells (Fig. 4 *B*). Second, no nonlinear charge movement is present in the range of our leak pulses (Fig. 4 *C*). Third, the measured charge movement is not affected by the choice of the leak subtraction protocols (data not shown). Finally, these "nonlinear displacement" currents have the standard properties typically associated with gating currents (Fig. 4 *D*): time integrals of outward (Q_{on}) and inward (Q_{off}) displacement currents saturated with increasing test depolarization; $Q_{off} \sim Q_{on}$ in the absence of inactivation (Fig. 4 *D*); charge movement (Q_{on}-V or Q_{off}-V curves) occurs before, and then parallels, ionic-current activation (G-V curve); and finally, the maximal amount of gating-charge (Q_{max}) is linearly correlated with maximal current density (G_{max}) (Fig. 4 *E*).

Mechanism of Current Potentiation by Auxiliary Subunits

With the ability to isolate gating currents, we could now compare auxiliary subunits with regard to their mechanism for current potentiation. Fig. 5 *A* displays representative gating-current records for most of the different subunit combinations. These traces illustrate that all auxiliary subunits boost the maximum amount of gating charge (Q_{max}), which is taken as the saturating value of the Boltzmann fit to the Q_{on}-V relation. Fig. 5 *B* compares the average values of Q_{max} for all different subunit combinations examined. Q_{max} for channels expressed from α_{1E} alone was characteristically small, with a mean of 0.8 ± 0.1 fC/pF (n = 9). β Subunits induced the strongest enhancement of Q_{max}, ranging from fourfold for β_3 to sevenfold for β_4. Coexpression of $\alpha_2\delta$ also produced clear augmentation of Q_{max}, though the effect was less potent than for β subunits. Table I summarizes the complete details of the analysis. Given that gating-charge per channel (q) does not appear to be affected by auxiliary subunits (Noceti et al., 1996), the rise in Q_{max} likely reflects an increase in the number of functional channels (n). Hence, our results indicate that the enhancement of current density by auxiliary subunits arises, at least in part, from an increase in the number of functional channels. Such an increase in the number of functional channels may reflect either improved processing and trafficking of α_{1E} channels (increasing total amount of α_{1E} protein), or an increase in the fraction of functional α_{1E} protein in the membrane (with no increase in total amount of α_{1E} protein) by the $\alpha_2\delta$ and β subunits.

To determine whether an increase in the maximal open probability ($P_{o,max}$) also contributes to higher ionic-current densities, we calculated the ratio G_{max}/Q_{max}, which is directly proportional to $P_{o,max}$, so long as auxiliary subunits do not alter permeation properties of the channel (as in Fig. 6 *D* and Noceti et al., 1996). Fig. 5 *C* shows that all β subunits approximately doubled G_{max}/Q_{max}, but $\alpha_2\delta$ left the ratio unchanged. Table I reports further details of the calculations. The data in Fig. 5 suggest that β subunits enhance α_{1E} current density by jointly increasing the number of functional channels (as reported by Q_{max}) and the maximal open probability (as reflected by G_{max}/Q_{max}). The enhancement of current by the $\alpha_2\delta$ subunit appears to be fundamentally different: there may be a pure increase in the number of functional channels, without change in $P_{o,max}$.

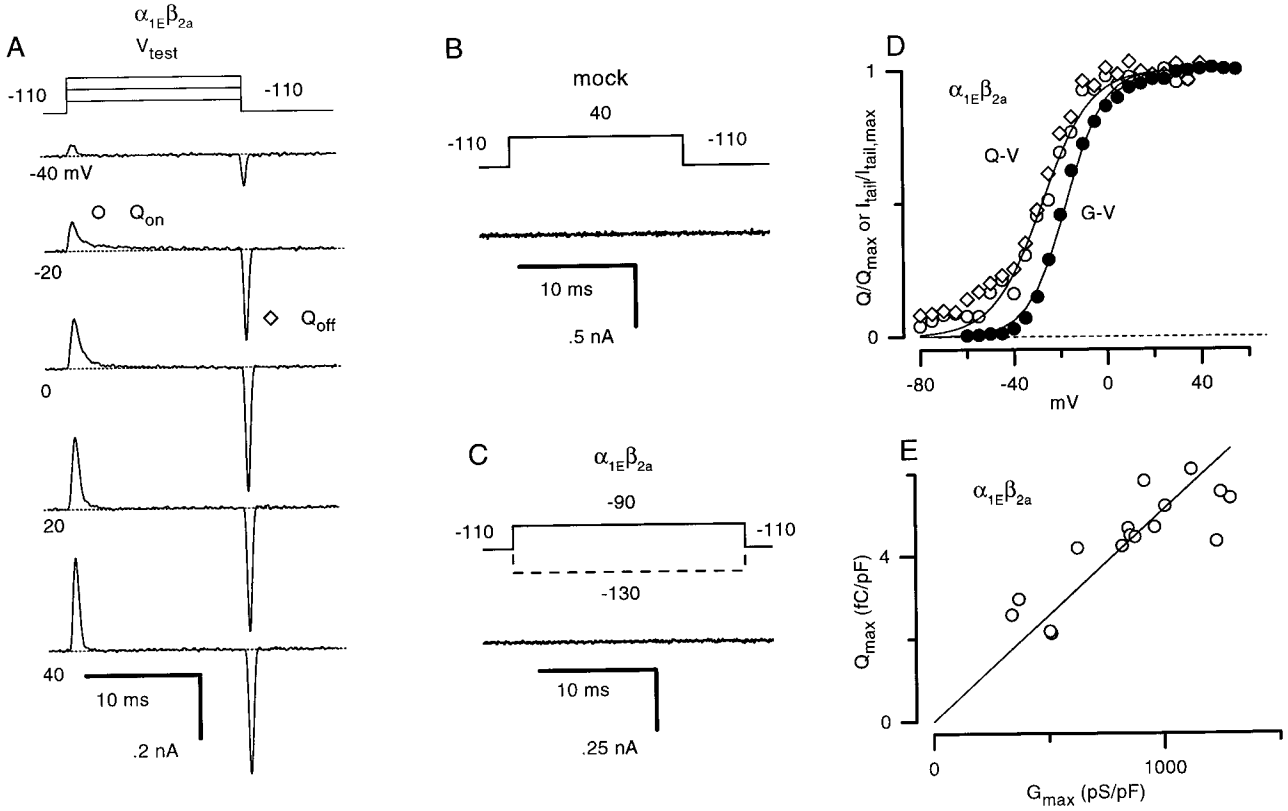

FIGURE 4. Isolation of α_{1E} gating currents. (*A*) Gating currents in response to the protocol used for measuring the voltage dependence of charge movement (Q-V). Representative traces are illustrated for an $\alpha_{1E}\beta_{2a}$-transfected cell (249_13) during ionic current blockade with 2 mM Mg^{2+}/0.2 mM La^{3+} for 15-ms test pulse depolarizations to −40, −20, 0, 20, and 40 mV from a holding potential of −110 mV. (*B*) Lack of gating current in a mock transfected cell (no α_{1E}), demonstrating the lack of appreciable amounts of endogenous voltage sensors. (*C*) Whole cell record in block solution from the cell in *A* in response to the indicated voltage protocol. The current trace is the difference of currents in response to positive and negative voltage jumps of opposite magnitudes, and illustrates that no nonlinear charge movement contaminates our leaks. (*D*) Charge movement occurs before activation of ionic currents. The voltage dependence of charge movement was derived by integrating the "ON" transient during depolarization (Q_{on}-V, ○) and the "OFF" transient during repolarization, respectively (Q_{off}-V, ◇), and normalizing by an estimate for the maximum amount of mobile charge. The ionic activation curve (G-V, ●) was derived from the voltage protocol in Fig. 2 *A* by normalizing peak tail currents (see MATERIALS AND METHODS). Solid lines represent the single-Boltzmann fits to the Q_{on}-V (fit parameters: $z = 2.7$, $V_{1/2} = -27.7$ mV) and to the G-V ($z = 3.1$, $V_{1/2} = -17$ mV). (*E*) Plot of ionic current density (G_{max}) versus the gating charge density (Q_{max}) for the cells used in calculating the G_{max}/Q_{max} ratio for $\alpha_{1E}\beta_{2a}$ (Table I). The plot illustrates the correlation between the magnitude of expressed current and mobile gating charge. Each data point represents one cell. Line is the identity relation.

Subunit Modulation of Activation Gating

A second goal of this study was to compare auxiliary subunit effects on the kinetics and voltage dependence of channel activation. To qualitatively compare activation kinetics for channels with different β subunits, we normalized the rising phases of exemplar ionic-current records (Fig. 2 *A*) evoked by voltage steps to −30, 10, and +10 mV (Fig. 6 *A*). The identical trajectories of traces from all four β subunits suggest that β subunits produce channels with similar activation kinetics. Fig. 6 *B* shows the identical analysis for channels expressed from α_{1E} alone (*solid trace*) or from $\alpha_{1E} + \alpha_2\delta$ (*dashed trace*). The records for $\alpha_{1E} + \beta_{1b}$ (*gray traces*) are reproduced for comparison. Here again, the close correspondence between traces suggests that auxiliary subunits do not significantly modulate activation kinetics.

To examine whether auxiliary subunits affect the steady state voltage dependence of activation (G-V), we tested for subunit-dependent changes in G-V curves derived from peak tail currents (see MATERIALS AND METHODS) (Fig. 6 *C*). Coexpression of the $\alpha_2\delta$ subunit had little effect on the G-V (Fig. 6 *C*) or I-V (Fig. 6 *D*) relations. The lack of effect of $\alpha_2\delta$ on the kinetics and voltage dependence of activation, as well as on G_{max}/Q_{max} (Fig. 5 *C*), suggests that this subunit is functionally uncoupled from any aspect of activation in α_{1E}. In contrast, single-Boltzmann function analysis (Fig. 6 *C, solid curves*, and Table II) clearly demonstrates that coex-

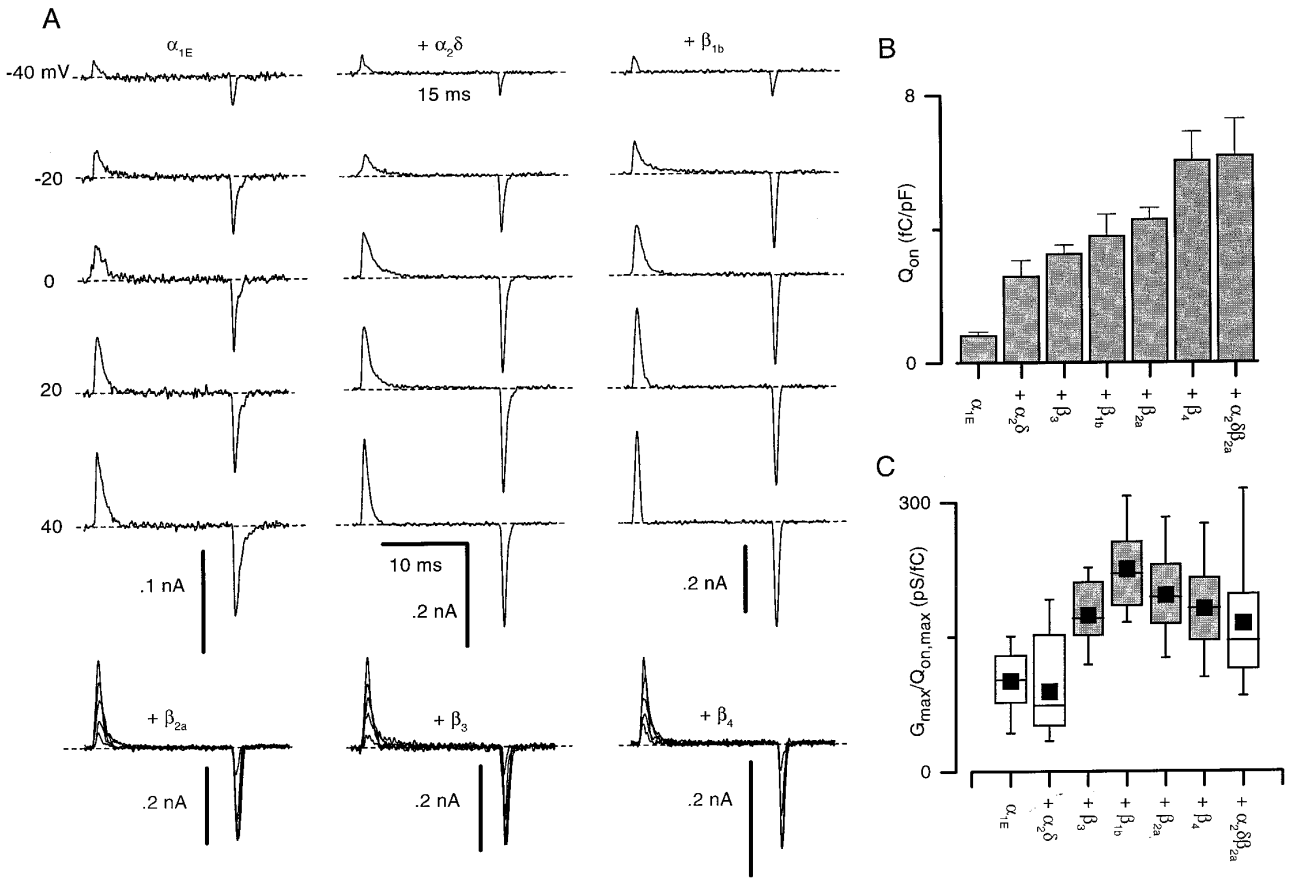

FIGURE 5. Comparison of gating currents for α_{1E} in combination with different auxiliary subunits. (*A*) Representative gating currents were obtained using the same voltage protocol and block solutions as in Fig. 4. Traces are for cells transfected with the indicated subunit combinations in response to test pulse voltages of −40, −20, 0, 20 and 40 mV, respectively. Same cells as in Fig. 2. (*B*) Comparison of the average Q_{max} values for different subunit combinations. The maximum amount of mobile charge (Q_{max}) was calculated from the saturating values of Boltzmann fits to Q_{on}-V. (*C*) Comparison of the average G_{max}/Q_{max} values for different subunit combinations. The maximum conductance (G_{max}) was determined from the saturating value of the Boltzmann fit to the tail-activation curves measured in 2 mM Ba^{2+}. Average G_{max}, Q_{max}, and G_{max}/Q_{max} values are summarized in Table I.

pression of β subunits produces an ~7-mV hyperpolarizing shift and a modest increase in the steepness of G-V relations (e.g., the Boltzmann valence (*z*) increases from 2.4 for α_{1E} to 3.6 for $\alpha_{1E}\beta_{2a}$). As expected from the shift in the G-V relation, coexpression of β subunits shifted the peak of the I-V relation leftward (Fig. 6 *D*) without altering the reversal potential.

The results in Fig. 6, *C* and *D,* are compatible with

TABLE I

Comparison of Subunit Effects on Current Density (G_{max}) and Charge Density (Q_{on}, Q_{off})

	n	G_{max}	I_{peak}	$Q_{on,max}$	$Q_{off,max}$	G_{max}/Q_{on}	G_{max}/Q_{off}
		pS/pF	*pA/pF*	*fC/pF*	*fC/pF*	*pS/fC*	*pS/fC*
α_{1E}	9	−82 ± 11	−2.9 ± 0.3	0.8 ± 0.1	−0.8 ± 0.1	100 ± 12	110 ± 18
$\alpha_{1E}\alpha_2\delta$	15	−206 ± 53	−8.4 ± 2	2.6 ± 0.5	−2.3 ± 0.4	89 ± 14	94 ± 12
$\alpha_{1E}\beta_{2a}$	16	−845 ± 78	−23.9 ± 2.3	4.3 ± 0.3	−4.6 ± 0.4	195 ± 11	186 ± 10
$\alpha_{1E}\beta_4$	9	−1036 ± 156	−33.2 ± 5.1	6.1 ± 0.8	−5.1 ± 0.6	180 ± 18	203 ± 15
$\alpha_{1E}\beta_{1b}$	13	−820 ± 112	−25.6 ± 4.8	3.8 ± 0.6	−3.6 ± 0.7	225 ± 13	241 ± 12
$\alpha_{1E}\beta_3$	8	−550 ± 58	−17.6 ± 2.3	3.3 ± 0.2	−3.1 ± 0.3	173 ± 15	177 ± 10
$\alpha_{1E}\beta_{2a}\alpha_2\delta$	19	−943 ± 143	−28.6 ± 5.2	6.2 ± 1.1	−6.2 ± 0.9	164 ± 14	158 ± 13

G_{max}, Q_{on}, and Q_{off} are derived as the saturating values of the single-Boltzmann fits to I_{tail}-V, Q_{on}-V, and Q_{off}-V data, respectively, normalized by the cell capacitance. I_{tail} corresponds to the peak tail current during repolarization to −50 mV with 2 mM Ba^{2+}. Q_{on} and Q_{off} are given by the integral of the ON and OFF gating current transients, respectively, measured in 2 mM Mg^{2+}/0.2 mM La^{3+}.

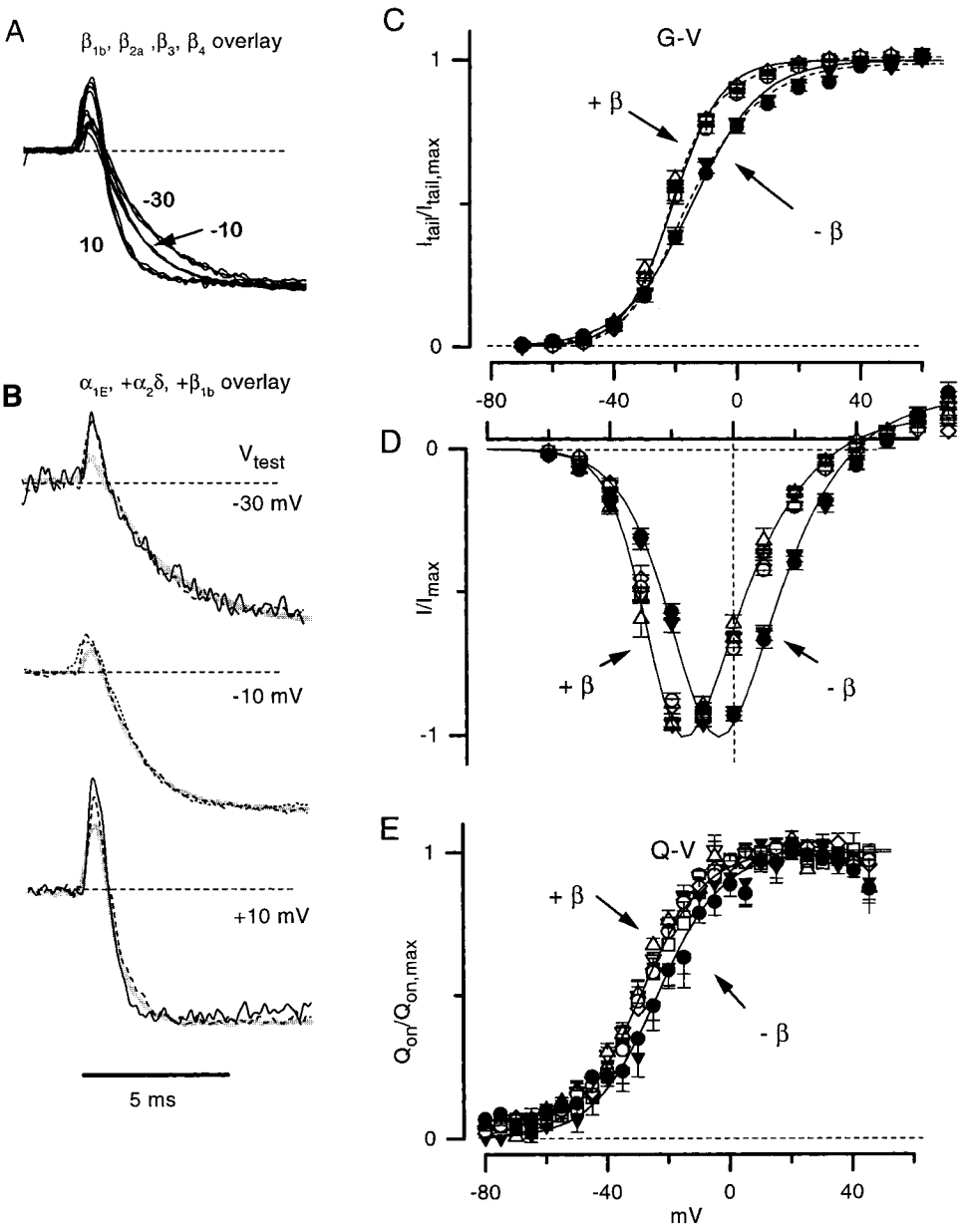

FIGURE 6. Effects of auxiliary subunits on the kinetics and voltage dependence of activation. (*A*) Comparison of activation kinetics for channels containing different β subunits. Ionic currents recorded in 2 mM Ba^{2+} for α_{1E} in combination with either β_{1b}, β_{2a}, β_3, or β_4 (cells 296_4, 252_5, 306_21, and 296_25, respectively) were scaled and superimposed for test pulse potentials of −30, 10, and 30 mV to illustrate activation kinetics. (*B*) Effect of addition of a β or the $\alpha_2\delta$ on activation kinetics. Ionic currents for α_{1E} (cell 171_3, *solid line*), $\alpha_{1E}\alpha_2\delta$ (cell 174_3, *dashed line*), and $\alpha_{1E}\beta_{1b}$ (cell 296_4, *gray line*) were scaled and superimposed for test pulse voltages of −30, −10, and 10 mV. (*C*) Averaged G-V relations for all the different subunit combinations (α_{1E}, ▼; $+\alpha_2\delta$, ●; $+\beta_{1b}$, □; $+\beta_{2a}$, ◇; $+\beta_3$, ▽; $+\beta_4$, △; $+\beta_{2a}\alpha_2\delta$, ○). This key applies to *D* and *E* also. G-V curves were derived using the protocol in Fig. 2 by normalizing peak tail currents during repolarization to −50 mV by an estimate for the maximal tail current (MATERIALS AND METHODS). The continuous curves represent single-Boltzmann fits to the averaged α_{1E} and $\alpha_{1E}\beta_{2a}$ data, with fit parameters ($z = 2.3$, $V_{1/2} = -14.6$ and $z = 3.3$, $V_{1/2} = -20.8$, respectively). Dashed curves represent dual-Boltzmann fits to the averaged α_{1E} and $\alpha_{1E}\beta_{2a}$ data with parameters ($V_{low} = -23.3$, $z_{low} = 4.3$, $V_{high} = -10.5$, $z_{high} = 2.1$, with the fraction of the low threshold component equal to 0.29 for α_{1E} and 0.71 for $\alpha_{1E}\beta_{2a}$). (*D*) Averaged current voltage relations for the same cells as in *C*. I-V relations for individual cells were normalized by the peak current before averaging. (*E*) Voltage dependence of charge movement for all the different subunit combinations. Q-V relations were derived using the protocol in Fig. 4 *A* by integrating the ON transient and normalizing by an estimate for the maximum amount of mobile charge ($Q_{on,max}$, see MATERIALS AND METHODS) before averaging across cells. Solid lines correspond to single-Boltzmann fits to α_{1E} data ($z = 2.4$, $V = -23.7$ mV) and to $\alpha_{1E}\beta_{2a}$ data ($z = 2.5$, $V = -29$ mV). Values are summarized in Table II.

earlier work on β subunit effects in *Xenopus* oocytes (Olcese et al., 1994), in which G-V relations were fitted with dual-Boltzmann functions. In agreement with the earlier report, application of dual-Boltzmann analysis to our G-V data (Fig. 6 *C, dashed curves*) suggests that the apparent hyperpolarization and steepening of activation by β subunits could arise from an increase in the proportion of the low threshold Boltzmann component from ~30 to ~70%, without change in valence or midpoint parameters of individual Boltzmann functions. More in-depth interpretation of the data, like that introduced by dual-Boltzmann analysis, is deferred to the DISCUSSION, where explicit fits of a multistate kinetic model will be employed. For simplicity, in the remainder of the RESULTS, we retain single-Boltzmann analysis for first-order characterization of experimentally resolvable changes in activation. Regardless of the particular analytical functions used to describe the data, the

TABLE II

Comparison of Average Boltzmann Fit Parameters for both the Voltage Dependence of Ionic Activation (G-V) and Charge Movement (Q-V)

channel	G-V	I_{tail}	G-V $V_{1/2}$	GV	Q-V	Q_{on}	Q_{on} $V_{1/2}$	Q_{on}	Q_{off}
	n	*pA*	*mV*	*z*	*n*	*fC*	*mV*	*z*	*fC*
α_{1E}	9	−210 ± 20	−14.9 ± 2.6	2.4 ± 0.1	8	80 ± 40	−23.4 ± 2.2	2.8 ± 0.2	−85.6 ± 46
$\alpha_{1E}\alpha_2\delta$	15	−733 ± 155	−12.8 ± 1.7	2.5 ± 0.2	12	119 ± 18	−23.3 ± 1.9	2.6 ± 0.2	−98.2 ± 19
$\alpha_{1E}\beta_{2a}$	19	−2419 ± 249	−21.3 ± 1.0	3.6 ± 0.1	25	200 ± 25	−29.0 ± 1.2	2.8 ± 0.1	−217.8 ± 22
$\alpha_{1E}\beta_4$	11	−2283 ± 382	−22.6 ± 1.2	3.1 ± 0.1	9	184 ± 26	−31.0 ± 1.1	2.5 ± 0.2	−155.9 ± 19
$\alpha_{1E}\beta_{1b}$	22	−1731 ± 223	−20.9 ± 0.4	3.1 ± 0.1	10	137 ± 42	−27.6 ± 1.7	2.8 ± 0.2	−119.6 ± 34
$\alpha_{1E}\beta_3$	17	−1436 ± 179	−21.2 ± 0.6	3.2 ± 0.1	7	165 ± 14	−31.6 ± 1.2	2.5 ± 0.1	−127.4 ± 14
$\alpha_{1E}\beta_{2a}\alpha_2\delta$	31	−2572 ± 221	−20.4 ± 0.9	3.3 ± 0.1	27	279 ± 52	−29.5 ± 1.2	2.8 ± 0.1	−277.3 ± 50

G-V relations were derived by measuring peak tail currents in 2 mM Ba^{2+} and Q-V relations were derived by integrating the ON gating current transient measured in 2 mM Mg^{2+}/0.2 La^{3+}. The fit function is described in MATERIALS AND METHODS.

results thus far (Figs. 5 and 6, *A–D*) clearly indicate that β subunits increase ionic current by simultaneously modulating the G-V relation and doubling the G_{max}/Q_{max} ratio, in agreement with the findings of Olcese et al. (1994, 1996).

To explore the mechanistic basis of the β subunit effects on activation, we investigated how auxiliary subunits influenced Q-V curves derived from gating currents (Fig. 6 *E*). The rising phase of Q-V curves is very sensitive to modulation of the early events in the activation pathway, and the interrelation of Q-V and G-V curves lends insight into steps that couple voltage sensor movement to channel openings (Jones et al., 1997*a*). Fig. 6 *E* illustrates that all β subunits produced essentially identical effects on the Q-V relation: a small hyperpolarizing shift in the midpoint (∼5 mV) with little change in the steepness (Boltzmann valence [*z*] ranges from 2.5 to 2.8, Table II). The effects of β subunits on Q-V curves are smaller than on G-V curves, thereby narrowing the gap between Q-V and G-V relations along the voltage axis. As expected from previous null results, $\alpha_2\delta$ had no effect on the Q-V relation. All the β subunit effects on gating (Figs. 5 *C* and 6, *C–E*), particularly the contraction between Q-V and G-V curves, fit nicely with the idea that all β subunits act primarily to modulate a single locus of weakly voltage-dependent steps late in the activation pathway (see DISCUSSION).

Functional Stoichiometry of β Subunit Interaction

Previous reports in *Xenopus* oocytes indicate that α_{1E} channels containing different β subunits have strikingly different inactivation characteristics, despite very similar activation gating (Olcese et al., 1994). Here, we sought to confirm this effect in HEK 293 cells so that we could exploit this property to test whether multiple β subunits can simultaneously define the functional behavior of a calcium channel. To assay inactivation properties, we used a 20-s prepulse followed by a test pulse to the peak of I-V relations (Fig. 7 *A*). Typical currents for $\alpha_{1E}\beta_{2a}$ and $\alpha_{1E}\beta_3$ channels illustrate the extremes of inactivation behavior observed with the different subunit combinations. β_{2a} dramatically slowed inactivation, while β_3 accelerated inactivation. β_{1b} and β_4 subunits also accelerated inactivation during the test pulse (not shown), though not as strongly as β_3. To provide a robust indication of the differences in inactivation properties, we used such records to calculate steady state inactivation curves (h(∞)V curves; Fig. 7 *B*). While addition of $\alpha_2\delta$ did not affect the h(∞)V relation, coexpression of β subunits induced striking modulation of steady state inactivation: β_{1b}, β_3, and β_4 all left-shifted h(∞)V curves by ∼10, 15, and 10 mV, respectively; β_{2a} imparted a right shift of ∼15 mV. The profound distinction between the effects of β_{2a} and the other β subunits has been reported in previous studies of α_{1E} (Olcese et al., 1994), and of other neuronal calcium channels, including α_{1A} (Stea et al., 1994) and α_{1B} (Patil et al., 1998). Table III summarizes the Boltzmann analysis of h(∞)V data.

To investigate whether multiple β subunits can concomitantly specify the functional properties of a single calcium channel, we took advantage of the vast difference between the h(∞)V relations for $\alpha_{1E}\beta_3$ and $\alpha_{1E}\beta_{2a}$ channels. If there are multiple β subunit sites on α_{1E} that specify inactivation properties, then cotransfection of both β_{2a} and β_3 subunits should result in mixed-composition channels (e.g., $\alpha_{1E}\beta_{2a}\beta_3$) whose inactivation behavior should be distinct from that of pure $\alpha_{1E}\beta_{2a}$- or $\alpha_{1E}\beta_3$-like channels. However, if there is only one functionally active β subunit site per channel, the aggregate h(∞)V relation should possess only two components. Fig. 8, *A* and *B*, shows the results for one such experiment in which β_3 and β_{2a} were cotransfected in a 1:1 weight ratio. This example demonstrates that inactivation is clearly biphasic, with a low threshold, readily inactivating component, as well as a high threshold, inactivation-resistant component. Only two Boltzmanns are

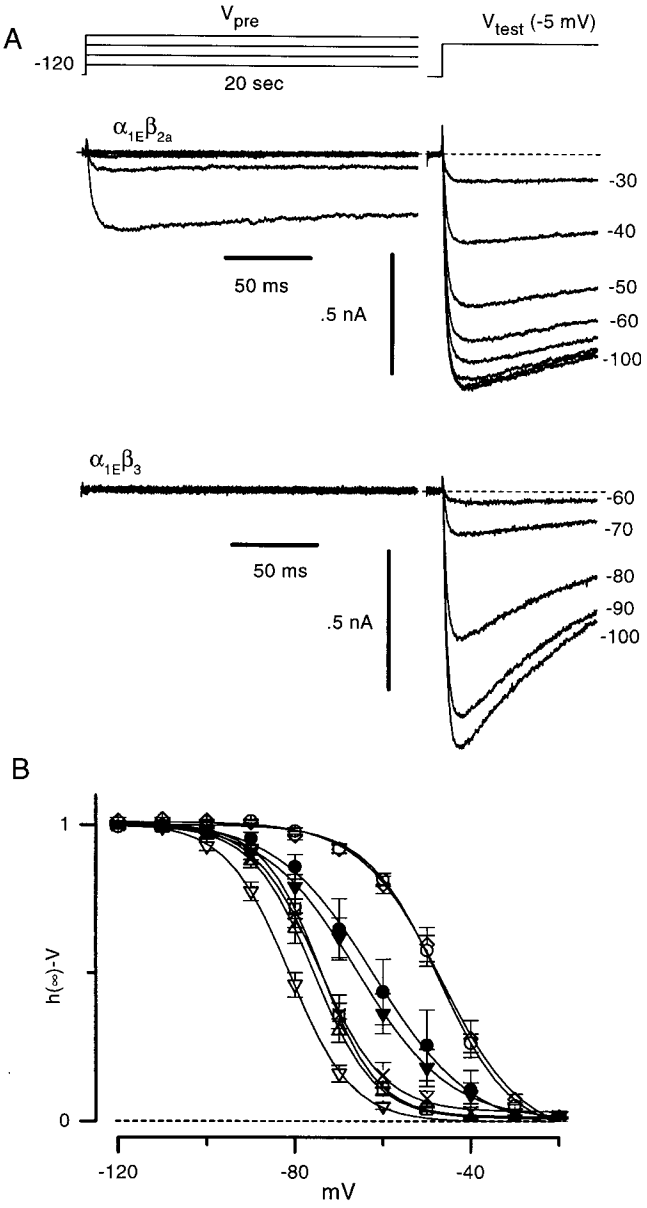

FIGURE 7. Auxiliary subunits modulate inactivation. (*A*, *top*) Voltage protocol used to approximate the steady state inactivation (h(∞)-V) relation. Voltage commands were given from a holding potential of −120 mV every 60 s. The test pulse potential was chosen to be the peak of the I-V relation, typically −5 mV. All h(∞)-V measurements were made with 10 mM Ba^{2+} as a charge carrier unless otherwise indicated. (*bottom*) Representative whole-cell records for a cell transfected with $\alpha_{1E}\beta_{2a}$ (cell 325_19) and a cell transfected with $\alpha_{1E}\beta_3$ (cell 327_11) for prepulse potentials of −100 to −30 mV (β_{2a}) and −100 to −60 mV (β_3), respectively. Only the first 200 ms of the prepulse were acquired and displayed. (*B*) Average h(∞)-V relations derived by normalizing the peak test pulse current data from the protocol in *A* by the peak test pulse current in the absence of a prepulse and averaging across cells. All subunit combinations are plotted, with the identical legend as in Fig. 6, with the addition of $\alpha_{1E}\beta_3\alpha_2\delta$ (×). Solid lines represent single-Boltzmann fits with values {subunit combinations [*z*, $V_{1/2}$ (mV)]}: α_{1E} (2.4 , −66), $+\alpha_2\delta$ (2.3, −62), $+\beta_{1b}$ (3.9, −74), $+\beta_{2a}$ (2.8, −46), $+\beta_3$ (3.6, −81.3), $+\beta_4$ (3.7, −75), $+\beta_{2a}\alpha_2\delta$ (3.2, −47), and $+\beta_3\alpha_2\delta$ (3.5, −74). Average fit values are summarized in Table III.

TABLE III

Comparison of Average h(∞)-V Fit Parameters for α_{1E} and $\alpha_{1E\Delta}$

	n	$V_{1/2}$	*z*
		mV	
α_{1E}	10	−65.7 ± 2.8	−3.0 ± 0.1
$\alpha_{1E}\alpha_2\delta$	9	−64.2 ± 4.7	−3.2 ± 0.1
$\alpha_{1E}\beta_{2a}$	12	−50.6 ± 1.5	−3.7 ± 0.1
$\alpha_{1E}\beta_4$	6	−75.7 ± 1.4	−3.7 ± 0.1
$\alpha_{1E}\beta_{1b}$	9	−73.8 ± 1.2	−4.0 ± 0.2
$\alpha_{1E}\beta_3$	7	−81.4 ± 1.2	−3.7 ± 0.2
$\alpha_{1E}\beta_{2a}\alpha_2\delta$	11	−48.7 ± 1.3	−3.4 ± 0.2
$\alpha_{1E}\beta_3\alpha_2\delta$	7	−74.3 ± 2.1	−3.3 ± 0.2
$\alpha_{1E\Delta}\alpha_2\delta$	13	−56.5 ± 2	−3.2 ± 0.1
$\alpha_{1E\Delta}\alpha_2\delta\beta_{2a}$	6	−38.9 ± 2.1	−3.2 ± 0.3
$\alpha_{1E\Delta}\alpha_2\delta\beta_3$	7	−71.0 ± 1.2	−3.8 ± 0.2
$\alpha_{1E\Delta}\beta_3$	4	−75.8 ± 2.3	−4.4 ± 0.1

For each cell, a single-Boltzmann was fit to the I_{peak}-V_{pre} relation, where I_{peak} is the test pulse current after a 20-s prepulse to V_{pre} (Fig. 7). Measurements were made in 10 mM Ba^{2+}. The fit function is given in MATERIALS AND METHODS.

required to produce an excellent fit of the data since the average residual for the dual-Boltzmann fit is close to zero (Fig. 8 *C*). Furthermore, the average fit parameters to the h(∞)V data correspond closely to the steady state inactivation properties of pure $\alpha_{1E}\beta_{2a}$ and $\alpha_{1E}\beta_3$ channels (Fig. 7 *B* and Tables III and IV). Cotransfection of β_3 and β_{2a} in a 5:1 weight ratio merely decreased the relative amplitude of the low threshold component (Fig. 8 *D*), while preserving the intrinsic properties of the two components (Table IV). The only apparent deviation from parameters obtained with pure-composition channels is a small 7–9-mV increase in the $V_{1/2}$ for the high threshold component (compare Tables III and IV). Although this increase could reflect a minor contribution of mixed-composition channels, the overall results are consistent with the functional dominance of pure $\alpha_{1E}\beta_{2a}$ and $\alpha_{1E}\beta_3$ channels.

As a further test for the possible functional role of a second β subunit site (Tareilus et al., 1997), we examined how auxiliary subunits modulated the properties of a COOH-terminal truncation of the α_{1E} construct ($\alpha_{1E\Delta}$, amino acids 1–1871 of α_{1E} [1–2251]) that lacks the secondary binding site. Fig. 9 *A* displays ionic currents for channels composed of $\alpha_{1E\Delta}+\alpha_2\delta$ or $\alpha_{1E}+\beta_{2a}+\alpha_2\delta$ subunits. Coexpression of β_{2a} with $\alpha_{1E\Delta}$ increased G_{max} from −306 ± 115 pS/pF (n = 11) to −1,708 ± 251 pS/pF (n = 4), a 5.6-fold increase similar to the 4.1-fold increase in G_{max} seen for wild-type α_{1E} (Fig. 2 *B*). Similarly, modulation of activation by β_{2a} is unchanged by the COOH-terminal deletion, as demonstrated in Fig. 9 *B* by the identical subunit modulation of G-V relations for $\alpha_{1E\Delta}$ (*circles*) and wild-type α_{1E} (*squares*). Finally, we compared β subunit modulation of the steady

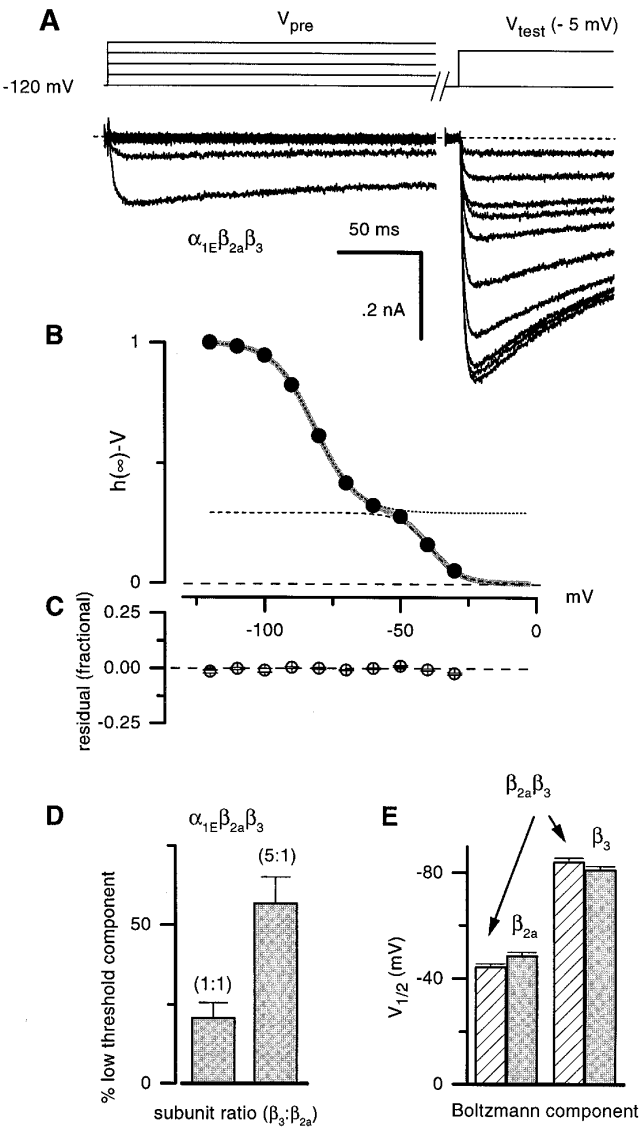

FIGURE 8. Simultaneous cotransfection of two β subunits (β_{2a} and β_3) leads to two distinguishable channel populations. (*A*) Current traces recorded in 10 mM Ba^{2+} in response to the same h(∞)-V protocol as in Fig. 7 (*top*), for a cell (330_18) transfected with α_{1E} in combination with equal amounts of β_{2a} and β_3. Traces displayed are for prepulse potentials ranging from −120 to −30 mV in 10–mV increments. (*B*) Plot of peak test-pulse currents (●) for the cell in *A*, illustrating the bimodal nature of inactivation. The thick line corresponds to a dual-Boltzmann fit to the data with parameters (low: −397 pA, $z = -3.4$, $V_{1/2} = -81.2$ mV; high: −164 pA, $z = -4.7$, $V_{1/2} = -39$ mV), in good correspondence with the average steady state inactivation properties of $\alpha_{1E}\beta_3$ and $\alpha_{1E}\beta_{2a}$ channels, respectively (Table III). The dotted and dashed lines illustrate the two components of the dual-Boltzmann fit. (*C*) Plot of average residuals ($n = 26$). The difference between the data and the fit value was normalized by the peak test-pulse current before averaging across cells. (*D*) Bar graph illustrating the dependence of the fraction of the low threshold Boltzmann component on the ratio of transfected β_{2a} and β_3. For the 1:1 ratio, $n = 17$, and for the 5:1 ratio, $n = 9$. (*E*) Comparison of average $V_{1/2}$ derived from dual-Boltzmann fits to the h(∞)-V for $\beta_{2a}\beta_3$-transfected cells (*diagonal striped*), with the average fit values derived from single-Boltzmann fits to h(∞)-V data for β_{2a}- or β_3-transfected cells (*gray*). Fit values and cell numbers are summarized in Table III (for β_{2a} or β_3 alone) and Table IV (for $\beta_{2a}\beta_3$-transfected cells).

state inactivation properties of $\alpha_{1E\Delta}$ (Fig. 9, *C, traces,* and *D, symbols*; Table III) with data obtained with wild-type α_{1E} (Fig. 9 *D, lines*). The α_{1E} data have been shifted uniformly by −7 mV in the Fig. 9 *D* overlay to account for a difference in inactivation that is present even without β subunit coexpression (e.g., $\alpha_{1E\Delta} + \alpha_2\delta$ in Fig. 9 *D*); this small shift likely reflects a difference in the intrinsic inactivation behavior of the α_1 backbone (Soldatov et al., 1997), rather than a change in the modulatory action of β subunits. The close correspondence between h(∞)-V relations for α_{1E} (*lines*) and $\alpha_{1E\Delta}$ (*symbols*) in the Fig. 9 *D* overlay illustrates that β subunit modulation of inactivation is similar for the two constructs. Although the small difference between modulation of $\alpha_{1E\Delta}$ and α_{1E} inactivation (most apparent for $\alpha_{1E\Delta}\beta_3\alpha_2\delta$, Fig. 9 *D*, ▽) could reflect a minor contribution of a second β subunit binding site, all the results in Figs. 8 and 9 support the view that a single β subunit binding site predominates in specifying inactivation properties. If present, the potential contribution of a second site appears to be small by comparison.

DISCUSSION

Although auxiliary subunits clearly have a role in defining channel properties, specific modulatory effects vary widely across studies, underscoring the need to examine comprehensively the modulation of each α_1 subunit under the same experimental conditions. Here, we have performed a systematic evaluation of auxiliary subunit regulation of expression and gating of α_{1E} calcium channels in HEK 293 cells. The experiments lead to three main conclusions. (*a*) The $\alpha_2\delta$ and β auxiliary subunits differ fundamentally in the manner by which they induce an overall increase in current density. Coexpression of $\alpha_2\delta$ with the pore-forming α_{1E} moiety produced a clear-cut enhancement of current, arising purely from an increase in the number of functional channels (n), without significantly affecting channel gating behavior. By contrast, coexpression of β subunits induced stronger potentiation of current by joint elevation of channel number (n) and maximal open probability ($P_{o,max}$), suggesting effects on both channel assembly and gating. (*b*) While $\alpha_2\delta$ had no appreciable effect on activation gating, β subunits produced significant hyperpolarizing shifts in the voltage dependence of ionic-current activation and gating-charge movement, all without discernible change in activation kinetics. Importantly, different β isoforms produced nearly indistinguishable effects in regard to both current potentiation and activation gating. (*c*) Little functional evi-

TABLE IV

Average Values for Dual-Boltzmann Fits to h(∞)-V Data for Cells Transfected with both β_{2a} and β_3 Simultaneously

	n	Percent low	$V_{1/2,low}$	$z_{1/2,low}$	$V_{1/2,high}$	$z_{1/2,high}$
			mV		*mV*	
$\alpha_{1E}\beta_{2a}\beta_3$ (1:1)	17	21 ± 5	−85.6 ± 2.1	−3.7 ± 0.3	−44.5 ± 1.2	−4.0 ± 0.3
$\alpha_{1E}\beta_{2a}\beta_3$ (1:5)	8	57 ± 8	−85.1 ± 1.3	−3.9 ± 0.2	−41.6 ± 1.4	−3.8 ± 0.3
$\alpha_{1E}\beta_{2a}\beta_3$ (all)	25	32 ± 5	−85.4 ± 1.3	−3.8 ± 0.2	−43.6 ± 1.0	−3.9 ± 0.2

The h(∞)-V relation was derived from peak test pulse currents after a 20-s prepulse. Fit function is described in MATERIALS AND METHODS.

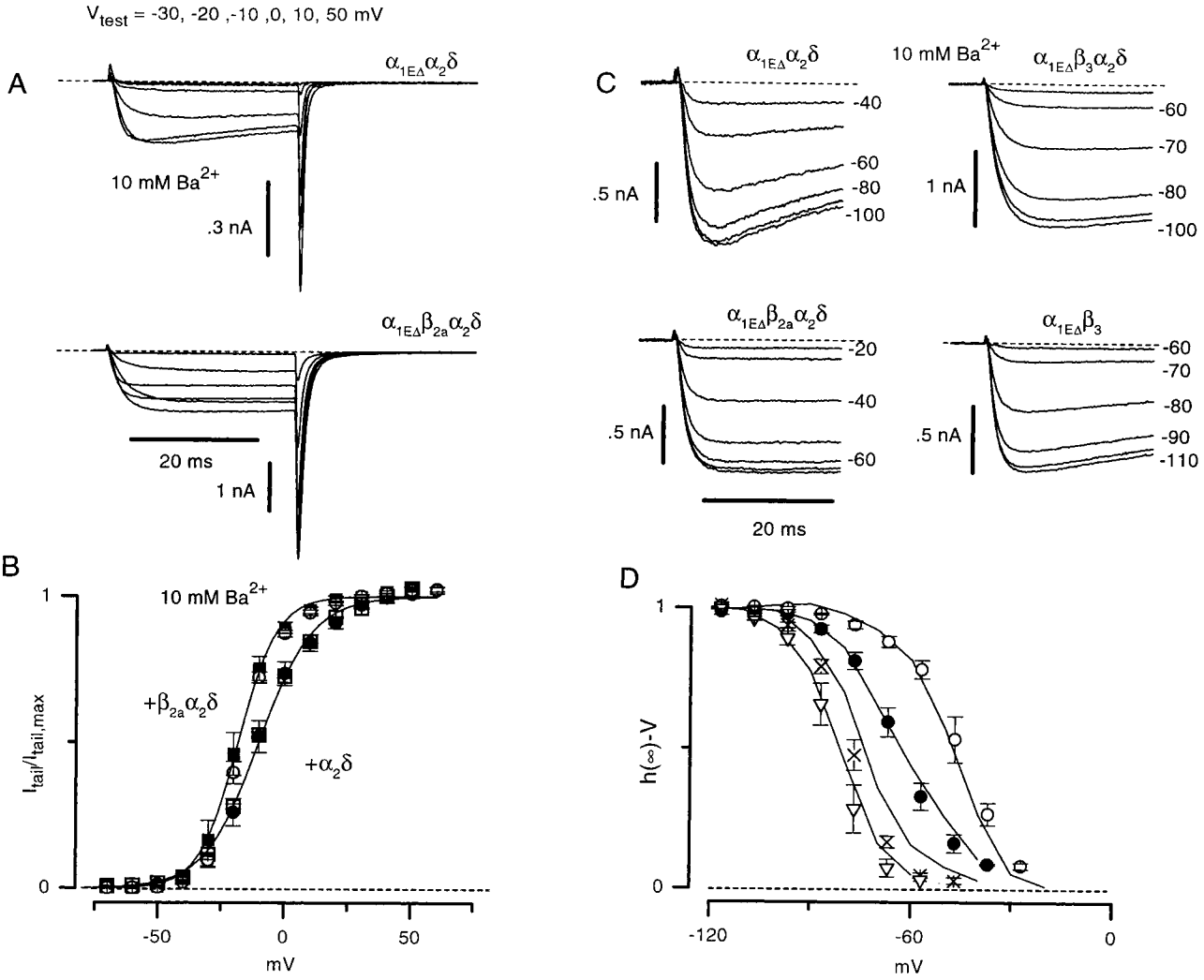

FIGURE 9. Activation and inactivation properties of a COOH-terminal truncated version of α_{1E} ($\alpha_{1E\Delta}$, amino acids 1–1871) that lacks a putative β binding site. All measurements for both α_{1E} and $\alpha_{1E\Delta}$ are in 10 mM Ba^{2+}. (*A*) Traces illustrating activation of ionic currents for $\alpha_{1E\Delta}\alpha_2\delta$ (cell 375_19) or $\alpha_{1E\Delta}\beta_{2a}\alpha_2\delta$ (cell 370_6) using the same voltage protocol as in Fig. 2. Data are shown for test pulse potentials of −30, −20, −10, 10, and 50 mV. (*B*) Comparison of G-V for $\alpha_{1E\Delta}$ and α_{1E} indicates that modulation of $\alpha_{1E\Delta}$ activation by β subunits is preserved. Symbols correspond to data for $\alpha_{1E\Delta}$ and wild-type α_{1E} ($\alpha_{1E\Delta}\beta_{2a}\alpha_2\delta$, ○, $n = 4$; $\alpha_{1E\Delta}\alpha_2\delta$, ●, $n = 11$; $\alpha_{1E}\alpha_2\delta$, ■, $n = 11$; and $\alpha_{1E}\beta_{2a}$, □, $n = 8$). Lines are single-Boltzmann fits to the $\alpha_{1E}\alpha_2$ and $\alpha_{1E}\beta_{2a}$ data with fit parameters $z = 2.4$, $V_{1/2} = -10.1$; and $z = 3.4$, $V_{1/2} = -18.2$, respectively. The shift in $V_{1/2}$ values relative to Fig. 6 *C* corresponds to a surface potential shift between 10 mM (used here) and 2 mM Ba^{2+} (Fig. 6). (*C*) Steady state inactivation. Traces after a 20-s prepulse (as in Fig. 7) to the indicated potentials are shown for $\alpha_{1E\Delta}$ in combination with $\alpha_2\delta$ (cell 376_9), β_3 (cell 375_4), $\beta_{2a}\alpha_2\delta$ (cell 370_11), and $\beta_3\alpha_2\delta$ (cell 371_10). (*D*) Comparison of h(∞)-V relations for $\alpha_{1E\Delta}$ (*symbols*) and α_{1E} (same data as in Fig. 7, shown as lines connecting mean data values, without explicit reproduction of data points as symbols). Symbols correspond to the following constructs: $\alpha_{1E\Delta}\alpha_2\delta$, ●; $\alpha_{1E\Delta}\beta_{2a}\alpha_2\delta$, ○; $\alpha_{1E\Delta}\beta_3$, ▽; $\alpha_{1E\Delta}\beta_3\alpha_2\delta$, ×. Data for α_{1E} is shifted by −7 mV to overlay the $\alpha_{1E\Delta}$ data. Average fit values and cell numbers are summarized in Tables V (G-V) and III [h(∞)-V] for both α_{1E} and $\alpha_{1E\Delta}$.

TABLE V

Comparison of Average Boltzmann Fit Values to G-V Relations for α_{1E} and $\alpha_{1E\Delta}$

	n	$I_{tail,max}$	G-V $V_{1/2}$	G-V
		pA	*mV*	*z*
$\alpha_{1E}\alpha_2\delta$	11	−550 ± 14	−10.2 ± 0.3	2.5 ± 0.1
$\alpha_{1E}\alpha_2\delta\beta_{2a}$	8	−3365 ± 437	−16.6 ± 1.2	3.7 ± 0.2
$\alpha_{1E\Delta}\alpha_2\delta$	11	−643 ± 203	−9.0 ± 1.8	2.7 ± 0.2
$\alpha_{1E\Delta}\alpha_2\delta\beta_{2a}$	4	−4622 ± 1066	−16.4 ± 0.9	3.5 ± 0.2

G-V relations were derived by measuring peak tail currents in 10 mM Ba^{2+} upon repolarization to −50 mV. The fit function is described in MATERIALS AND METHODS.

dence for a secondary β subunit binding site was found, fitting with earlier biochemical evidence for a 1:1 stoichiometry of α_1 and β subunits for skeletal (De Waard and Campbell, 1995) and neuronal N-type (Witcher et al., 1993) channels. Together, these findings represent an important contribution to clarifying both the mechanism and structural determinants of auxiliary-subunit modulation of calcium channels.

In the sections to follow, we will first relate each of the conclusions to previous studies of α_{1E} and, where relevant, other calcium channels. For clarity, we will discuss $\alpha_2\delta$ and β subunit effects sequentially, as independent parts. A kinetic mechanism is then developed to explain how β subunits can produce all the observed changes in gating, simply by alteration of the equilibrium between a single, weakly voltage-dependent transition near the open state. Finally, we consider the generality of our conclusions to other α_1 isoforms.

Modulation of α_{1E} by $\alpha_2\delta$

The $\alpha_2\delta$ subunit produced an approximately threefold increase in α_{1E} current, which arose almost exclusively from elevated channel expression (Q_{max}). The $\alpha_2\delta$ subunit had no other clear modulatory effects, except to slightly antagonize the effect of β_3 on inactivation (Fig. 7 *B*). All measures of activation gating, including the maximal open probability (G_{max}/Q_{max}), the voltage dependence of charge movement (Q-V), and the voltage dependence of ionic activation (G-V) were similar to α_{1E} alone. Similar effects on inactivation and expression were reported for doe1 (marine ray analog of α_{1E}) expressed in *Xenopus* oocytes (Ellinor et al., 1993). However, in contrast to our results, in studies of rat α_{1E} in COS-7 cells (Stephens et al., 1997) and human α_{1E} in *Xenopus* oocytes (Wakamori et al., 1994), coexpression of $\alpha_2\delta$ was found to produce a depolarizing shift in the G-V without modifying expressed current levels; however, these studies agree with our findings concerning the slight antagonism of β_3 effects on inactivation (Fig. 7 *B*).

The applicability of our results to other channel types is unclear. However, it is interesting to note that the reported effects of the $\alpha_2\delta$ subunit on other α_1 subunits also varies widely, sometimes agreeing with our findings, other times not. For example, with regard to modulation of α_{1C} channel density, the $\alpha_2\delta$ subunit was found to increase ligand binding sites (Welling et al., 1993), protein levels (Shistik et al., 1995), and gating currents (Bangalore et al., 1996). By contrast, in other studies (Wei et al., 1995; Gurnett et al., 1997) of α_{1C}, maximal dihydropyridine binding is not increased by $\alpha_2\delta$ coexpression. Similarly, activation kinetics of α_{1C} accelerate in some studies (Singer et al., 1991; Bangalore et al., 1996), but not others (Mikami et al., 1989; Welling et al., 1993). The sources of this variability have yet to be determined.

β Subunits Act Differently than the $\alpha_2\delta$ Subunit

By contrast to the $\alpha_2\delta$ subunit, coexpression of β subunits (β_1–β_4) enhanced current density (G_{max}) by increasing not only the number of functional channels (Q_{max}) but also the maximum open probability (G_{max}/Q_{max}). Similar effects on current density have been reported in COS 7 (Stephens et al., 1997) and HEK 293 cells (Williams et al., 1994), but not in *Xenopus* oocytes (Soong et al., 1993; Olcese et al., 1994, 1996). Furthermore, in a study of α_{1E} gating currents in *Xenopus* oocytes (Olcese et al., 1996), coexpression of β_{2a} with α_{1E} actually decreased the number of functional channels (Q_{max}), although surprisingly they found a twofold increase of G_{max}/Q_{max} that is qualitatively similar to our result. Additional support for the role of the β subunit in modulating $P_{o,max}$ comes from a separate study that used fluctuation analysis to determine the effects of β_{2a} and β_{1a} on α_{1E} open probability (Noceti et al., 1996).

Fitting with the doubling of the G_{max}/Q_{max} ratio, the β subunit also induced hyperpolarizing shifts of both G-V and the Q-V relations and slightly reduced the gap between the two, all while producing little effect on activation kinetics. Here, the action of β subunits is also somewhat controversial. Although most studies of α_{1E} report effects on G-V relations and activation kinetics that are similar to ours (Witcher et al., 1993; Olcese et al., 1994; Stephens et al., 1997), in one case (Wakamori et al., 1994), β_{1b} coexpression with the human α_{1E} in *Xenopus* oocytes was found to slow activation kinetics substantially. With respect to gating currents, the only other study of α_{1E} charge movement (Olcese et al., 1996) also found that the β subunit reduced the gap between the G-V and Q-V. However, in contrast to the small but statistically significant ($P < 0.01$, Student's *t* test, comparing cells with and without a β) shift in the Q-V reported here, Olcese et al. (1996) found that the β subunit produced no significant change in the Q-V. Again, these discrepancies may reflect differences between clones (human versus rat α_{1E}) or expression systems (*Xenopus* oocytes versus HEK 293 cells). Despite

these minor differences, all the results indicate a role for β subunits in modulating activation gating.

In other calcium channels, the reported effects of the β subunits vary even more widely than for the $\alpha_2\delta$ subunit. However, at least in some respects, β subunit modulation of other α_1 subunits appears similar to what we find for α_{1E}. For example, there are reported shifts in the voltage dependence of ionic activation for α_{1A} (Stea et al., 1994; De Waard and Campbell, 1995) and α_{1C} (Wei et al., 1991; Neely et al., 1993). Increased current density has also been observed for many of the α_1 subunits including α_{1A} (Mori et al., 1991), α_{1B} (Williams et al., 1992*a*), α_{1C} (Perez-Reyes et al., 1992), α_{1D} (Williams et al., 1992*b*), and α_{1S} (Ren and Hall, 1997). Furthermore, for α_{1C}, studies of gating currents in both HEK 293 cells (Kamp et al., 1996; Josephson and Varadi, 1996) and *Xenopus* oocytes (Neely et al., 1993) find that β subunit modulation of ionic current activation is not associated with much shift in the Q-V, similar to what we find for α_{1E}. On the other hand, even these few gating current studies disagree in other regards. While coexpression of β_{1a} (Kamp et al., 1996) or β_3 (Josephson and Varadi, 1996) with α_{1C} increased both current density and Q_{max} in HEK 293 cells similar to our results for α_{1E}, β_{2a} increased current without changing Q_{max} in *Xenopus* oocytes (Neely et al., 1993). Therefore, as with α_{1E}, the specific effects observed with β coexpression appear to depend on as yet unknown distinctions between expression systems, perhaps the endogenous expression of β_{XO} subunits in *Xenopus* oocytes (Tareilus et al., 1997).

Different β Isoforms Have Similar Effects on Activation and Expression, but Not on Inactivation

There was little isoform dependence to the modulation of all the above measures of activation gating, suggesting that different β subunits act by a similar mechanism to modulate activation and expression of α_{1E}, despite very different effects on inactivation. While no other study has compared gating currents of α_{1E} channels containing different β subunits, measurements of α_{1E} ionic-current G-V curves in *Xenopus* oocytes support this finding (Olcese et al., 1994). However, for other α_1 subunits, modulation of expression and activation may differ across β subunits. For example, there clearly is isoform specificity in the β subunit modulation of current potentiation in α_{1A} (Stea et al., 1994; De Waard et al., 1994) and α_{1S} (Ren and Hall, 1997). This fits with the binding affinity differences in vitro of various β subunits to α_{1A} (De Waard et al., 1995). However, binding of various β subunits to the I-II linker of α_{1B} occurs with the same affinity (Scott et al., 1996). Whether differences in in vitro binding affinities translates into discernible gradations of functional effects remains to be established.

One β Subunit May Predominate in Directing Baseline Channel Properties

Most previous studies have implicitly assumed that only one β subunit is involved in modulating channel properties, consistent with biochemical evidence for a 1:1 stoichiometry of α_1 and β subunits for skeletal (De Waard et al., 1996) and N-type (Witcher et al., 1993) channels. However, a recent report by Tareilus et al. (1997) identified a second β subunit binding site on the COOH terminus of α_{1E}, raising the possibility that two or more β subunits might collectively determine channel gating properties. Here, we found little evidence that two β subunits modulate the properties of the α_{1E} channel, either in regard to expression or gating.

Mechanism of β Subunit Modulation of α_{1E} Gating

To account for β subunit effects on G-V and Q-V curves, previous studies have proposed that the β subunit acts mainly on the weakly voltage-dependent steps that "couple" channel opening to voltage sensor movement (Neely et al., 1993; Olcese et al., 1996). Here, we demonstrate that this mechanism may explain not only the modulation of G-V and Q-V curves, but also the doubling of maximum open probability. Fig. 10 depicts a channel gating model that closely resembles those previously used in the study of potassium channel gating (Zagotta and Aldrich, 1990; Schoppa et al., 1992). There are three independent, voltage-dependent transitions between the closed states (C_0, C_1, C_2, and C_3), each associated with an appropriately scaled equilibrium constant K_0. These transitions are followed by a weakly voltage-dependent transition (C_2–C_3) with equilibrium constant K_1 and a final voltage-independent step with equilibrium constant K_2. K_0 and K_1 are voltage dependent according to a Boltzmann distribution, $K_i = \exp\{[z_i F(V - V_i)]/(RT)\}$. To obtain baseline model parameters (z_0, z_1, V_0, V_1, K_2), we fit α_{1E} alone Q-V and G-V data (Fig. 10 *B*). Then, to simulate the observed twofold change in the maximum open probability, we modified only K_2, the equilibrium constant for the last voltage-independent transition leading to channel opening. This simple change reproduced well both the shift in the G-V relationship and the shift in the Q-V relationship (Fig. 10 *C*). In fact, such simulations indicate that modifying the coupling of charge movement to channel opening (K_2) usually also perturbs the Q-V relation and, therefore, charge movement. Yet in several studies (Kamp et al., 1996; Josephson and Varadi, 1996; Neely et al., 1993; Olcese et al., 1996), shifts in ionic activation have been seen with little or no modification of charge movement. In these studies, it may be that the shift in charge movement is too small to be well resolved.

To determine the effect of modifying K_2 on the time course of activation, we modeled the kinetics of activa-

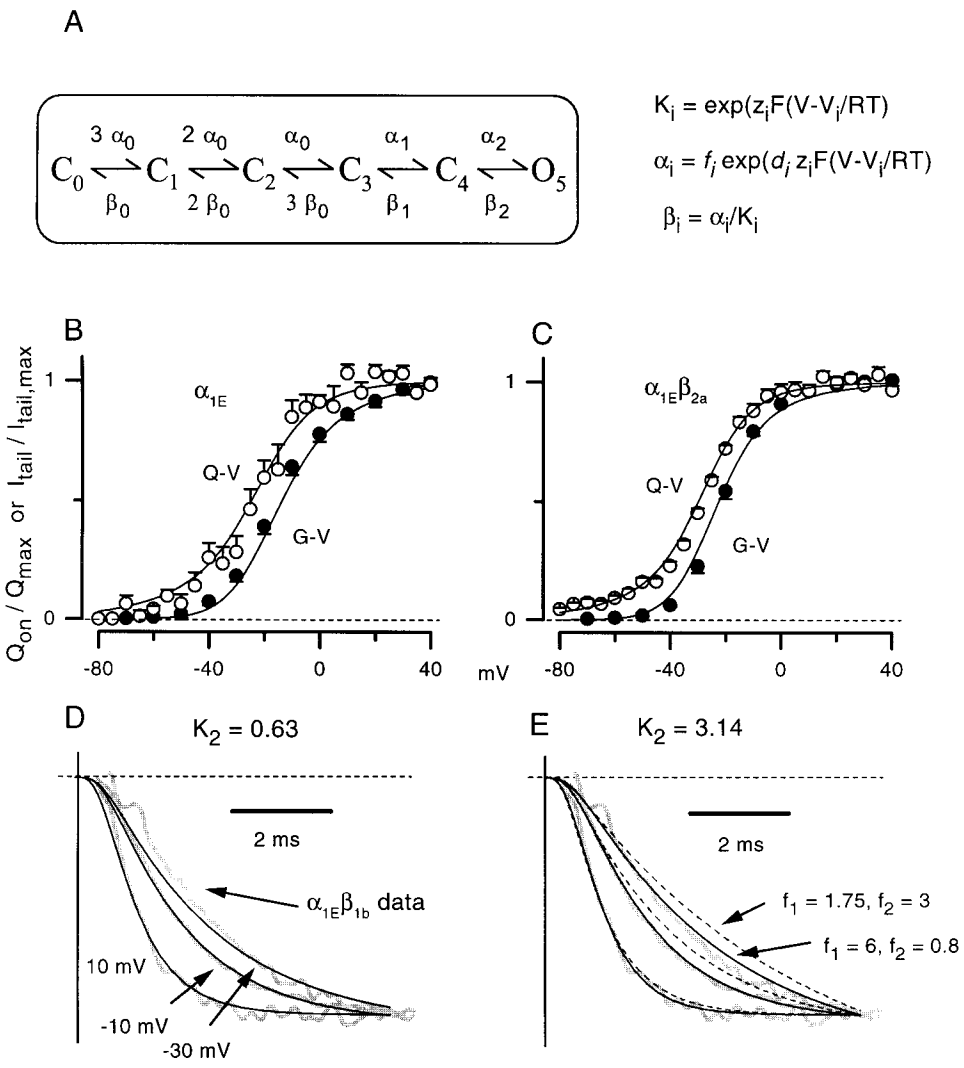

FIGURE 10. (*A*) Scheme used to model steady state activation. The equilibrium constant between two states is assumed to have the form $K_i = \alpha_i(V)/\beta_i(V) = \exp\{[z_i F(V - V_i)]/(RT)\}$, where $\alpha_i(V)$ and $\beta_i(V)$ are rate constants (millisecond^{-1}), z_i gives the valence of the gating charge moved in the transition, and V_i is related to the zero-potential free energy difference between the two states. Transitions through states C_0–C_3 correspond to Hodgkin-Huxley-like behavior of three identical gating particles, each characterized by the same equilibrium constant, K_0. The movement of the three gating particles is followed by a weakly voltage-dependent step, which has a separate equilibrium constant, K_1. Finally, there is a voltage-independent transition, with equilibrium constant K_2 ($z_2 = 0$). (*B*) Plot of the G-V (●) and Q-V (○) data from Fig. 6 for α_{1E}. The solid lines correspond to model fits with parameters: $z_0 = 1.32$, $V_0 = -15.2$ mV, $z_1 = 0.39$, $V_1 = -104$ mV, $K_2 = 0.63$. (*C*) Plot of the G-V (●) and Q-V (○) data from Fig. 6 for $\alpha_{1E}\beta_{2a}$. Solid lines are the model fits produced by changing K_2 for α_{1E} to 3.14, leaving all other equilibrium parameters the same. This change in K_2 corresponds to a 1.96-fold increase in the maximum open probability [$P_{o,max} = K_2/(K_2 + 1)$]. (*D*) Model fits for kinetics of activation. Pure ionic currents (*thick gray line*) were obtained for $V_{test} = -30$, -10, and 10 mV by subtracting gating currents measured in 2 mM Mg^{2+}/0.2 mM La^{3+} from the currents measured in 2 mM Ba^{2+} ($\alpha_{1E}\beta_{1b}$, cell 296_4, same cell as in Fig. 6 *A*). The solid line is the model fit with kinetic parameters ($f_0 = 1.8$, $d_0 = 0.4$, $f_1 = 1.75$, $d_1 = 0.5$, $f_2 = 3$) consistent with the steady state model parameters from *B* for α_{1E} alone. (*E*) The dashed line illustrates the kinetics that result when K_2 is changed from 0.63 to 3.14, while otherwise maintaining the same model parameters as in *D*. This effect may be offset by setting f_1 to 6 and f_2 to 0.8 (*solid line*). Note that it is not necessary to modify parameters for the early transitions (f_0, d_0) to obtain a reasonable fit.

tion. The choice of rate constants is constrained by the equilibrium constants, according to $K_i(V) = \alpha_i(V)/\beta_i(V)$, where $\alpha_i(V)$ is the forward rate constant and $\beta_i(V)$ is the backward rate constant (seconds^{-1}). We chose $\alpha_i(V) = f_i \exp\{[d_i z_i F(V - V_i)]/(RT)\}$, and $\beta_i(V) = \alpha_i(V)/K_i(V)$, giving us free parameters f_0, d_0, f_1, d_1, and f_2, which we could vary to fit the activation kinetics. Fig. 10 *D* shows a model fit (*thin solid line*) consistent with α_{1E} alone steady state model parameters (z_0, z_1, V_0, V_1, K_2; Fig. 10 *B*). Representative ionic current data (Fig. 10 *B*, *thick gray line*) are derived by subtracting the gating currents (Fig. 5 *A*) from the $\alpha_{1E}\beta_{1b}$ whole cell records in Fig. 6 *A*. Because of the subunit invariance of activation kinetics, these ionic currents also represent the expected time course of α_{1E} alone. Changing K_2 to accord with the twofold increase in maximal open probability produced by β subunits can modify the activation kinetics (Fig. 10 *E, dashed line*), but this may be compensated for by altering only f_1 and f_2. This amounts to subtle changes in the absolute rate constants of the last two transitions, but only an alteration of the equilibrium constant of the last transition. Although no change in parameters corresponding to the more voltage-dependent steps (z_0 and f_0) is necessary, we found that we could not well reproduce the invariance of activation kinetics by just modifying f_2, corresponding to the last voltage-independent step. Therefore, this simulation argues that all the effects of β subunit modulation of α_{1E} (increased open probability, hyperpolarization of G-V and Q-V curves, and invariant activation kinet-

ics) can be attributed to actions on one or a few weakly voltage-dependent steps before opening.

Generalizability of Results to Other α_1 Isoforms?

From the previous discussion, it is clear that generalization across α_1 subtypes is a difficult proposition. Nevertheless, we wondered whether some of the most robust properties of α_{1E} modulation by subunits would translate to a different α_1 subunit. In particular, there was striking adherence to two "rules" for α_{1E} modulation by subunits: (*a*) all β subunits produce no change in the kinetics of activation, but induce identical but relatively small hyperpolarizing shifts of the G-V curve, and (*b*) distinct β subunits impart vastly different steady state inactivation curves. Do these features of subunit modulation hold true as general tenets for other α_1 subunits?

Fig. 11 tests this proposition for the α_{1C} calcium channel. The results indicate a complete reversal of the behavior found with α_{1E}. Now the kinetics of activation are clearly different for β_3 and β_{2a} subunits. In addition, the different β isoforms led to large differences in G-V curves. On the other hand, steady state inactivation curves show only small isoform-dependent distinctions.

The diametrically opposite behaviors exhibited by α_{1E} and α_{1C} subunits have interesting implications for the structure–function relations underlying α_1-β modulation. The leading candidates for structural interaction between these two subunits are a small motif on the I-II linker of α_1 subunits known as the "alpha interaction domain" or AID (Pragnell et al., 1994), and another small motif in the middle of β subunits known as the "β interaction domain" or BID (De Waard et al.,

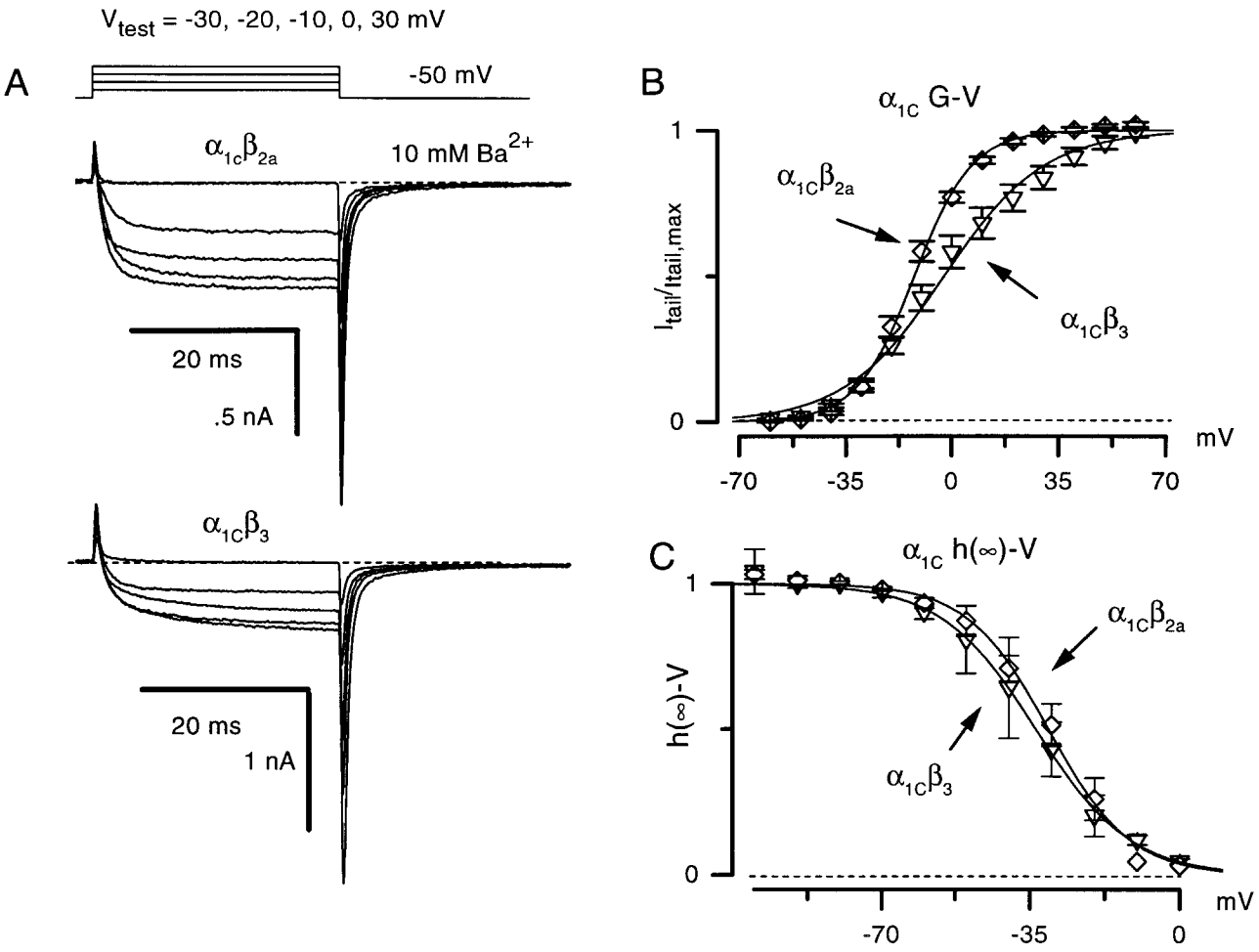

FIGURE 11. (*A*) Representative whole-cell records obtained using the same voltage protocol and ionic conditions as in Fig. 2, but now from cells transfected with either $\alpha_{1C}\beta_{2a}$ (cell 83_2, *top*) or $\alpha_{1C}\beta_3$ (cell 337_6, *bottom*). Traces are plotted for test pulse potentials of −30, −20, −10, 0, and 30 mV. Note the slow activation of $\alpha_{1C}\beta_3$ compared with $\alpha_{1C}\beta_{2a}$ channels. (*B*) Average G-V relations for $\alpha_{1C}\beta_{2a}$ ($n = 10$, ◇) and $\alpha_{1C}\beta_3$ ($n = 9$, ▽). The solid lines are Boltzmann fits to the $\alpha_{1C}\beta_3$ ($z = 1.55$, V = −2.53 mV) and $\alpha_{1C}\beta_{2a}$ ($z = 2.7$, V = −12.4 mV) data. (*C*) h(∞)-V relations using the protocol in Fig. 7 for $\alpha_{1C}\beta_3$ ($n = 2$–3, ▽) and $\alpha_{1C}\beta_{2a}$ ($n = 2$–3, ◇), with 10 mM Ba^{2+} external, using a different internal solution (see MATERIALS AND METHODS). Solid lines are Boltzmann fits to $\alpha_{1C}\beta_{2a}$ ($z = 2.7$, V = −30 mV), and $\alpha_{1C}\beta_3$ data ($z = 2.3$, V = −33 mV).

1995). AID and BID peptides bind with high affinity (tens of nanomolar), and the BID region has documented importance for modulation of α_1 subunits (De Waard et al., 1995). The key points with regard to our findings are that the BID is highly (~70%) homologous across β subunits, and the AID is also highly conserved across different α_1 subunits (Pragnell et al., 1994; De Waard et al., 1995). The profound differences in β isoform selectivity for entirely different gating properties, depending on the α_1 subtype, suggest that either the AID–BID interaction is exquisitely sensitive to small sequence variations in the AID (Scott et al., 1996), or there are other features that contribute to β subunit modulation of α_1 (Chien et al., 1996). Distinguishing between these two possibilities and identifying any secondary interaction sites will be important challenges for the future.

We thank K.P. Campbell for the β_{1b} clone, T.P. Snutch for the α_{1E} and $\alpha_2\delta$ clones, E. Perez-Reyes for the α_{1C}, β_{2a}, β_3, and β_4 clones, M. deLeon for construction of $\alpha_{1E\Delta}$, J.G. Mulle for technical assistance, and David Brody and Carla DeMaria for discussion and comments.

This work was supported by the National Institutes of Health (NIH) to D.T. Yue, the National Science Foundation Presidential Faculty Fellowship (D.T. Yue), a Maryland American Heart Association Postdoctoral Fellowship (S.K. Wei), and an NIH Medical Scientist Training Program Award (L.P. Jones).

Original version received 12 March 1998 and accepted version received 15 June 1998.

REFERENCES

Armstrong, C.M., and F. Bezanilla. 1974. Charge movement associated with the opening and closing of the activation gates of the Na channels. *J. Gen. Physiol.* 63:533–552.

Armstrong, C.M., and F. Bezanilla. 1977. Inactivation of the sodium channel. II. Gating current experiments. *J. Gen. Physiol.* 70:567–590.

Bangalore, R., G. Mehrke, K. Gingrich, F. Hofmann, and R.S. Kass. 1996. Influence of L-type Ca channel alpha 2/delta-subunit on ionic and gating current in transiently transfected HEK 293 cells. *Am. J. Physiol.* 270:H1521–H1528.

Bean, B.P., and E. Rios. 1989. Nonlinear charge movement in mammalian cardiac ventricular cells. Components from Na and Ca channel gating. *J. Gen. Physiol.* 94:65–93.

Bezanilla, F., E. Perozo, D.M. Papazian, and E. Stefani. 1991. Molecular basis of gating charge immobilization in *Shaker* potassium channels. *Science.* 254:679–683.

Brody, D.L., P.G. Patil, J.G. Mulle, T.P. Snutch, and D.T. Yue. 1997. Bursts of action potential waveforms relieve G-protein inhibition of recombinant P/Q-type Ca^{2+} channels in HEK 293 cells. *J. Physiol.(Camb.).* 499:637–644.

Castellano, A., X. Wei, L. Birnbaumer, and E. Perez-Reyes. 1993*a*. Cloning and expression of a neuronal calcium channel beta subunit. *J. Biol. Chem.* 268:12359–12366.

Castellano, A., X. Wei, L. Birnbaumer, and E. Perez-Reyes. 1993*b*. Cloning and expression of a third calcium channel beta subunit. *J. Biol. Chem.* 268:3450–3455.

Chien, A.J., K.M. Carr, R.E. Shirokov, E. Rios, and M.M. Hosey. 1996. Identification of palmitoylation sites within the L-type calcium channel beta2a subunit and effects on channel function. *J. Biol. Chem.* 271:26465–26468.

De Waard, M., and K.P. Campbell. 1995. Subunit regulation of the neuronal alpha 1A Ca^{2+} channel expressed in *Xenopus* oocytes. *J. Physiol. (Camb.).* 485:619–634.

De Waard, M., C.A. Gurnett, and K.P. Campbell. 1996. Structural and functional diversity of voltage-activated calcium channels. *In* Ion Channels. T. Narahashi, editior. Plenum Publishing Corp., New York. 41–87.

De Waard, M., M. Pragnell, and K.P. Campbell. 1994. Ca^{2+} channel regulation by a conserved beta subunit domain. *Neuron.* 13:495–503.

De Waard, M., D.R. Witcher, M. Pragnell, H. Liu, and K.P. Campbell. 1995. Properties of the alpha 1-beta anchoring site in voltage-dependent Ca^{2+} channels. *J. Biol. Chem.* 270:12056–12064.

Ellinor, P.T., J.F. Zhang, A.D. Randall, M. Zhou, T.L. Schwarz, R.W. Tsien, and W.A. Horne. 1993. Functional expression of a rapidly inactivating neuronal calcium channel. *Nature.* 363:455–458.

Gorman, C.M., D.R. Gies, and G. McCray. 1990. Transient production of proteins using an adenovirus transformed cell line. *DNA and Protein Engineering Techniques.* 2:3–10.

Gurnett, C.A., R. Felix, and K.P. Campbell. 1997. Extracellular interaction of the voltage-dependent calcium channel alpha-2 delta and alpha1 subunits. *J. Biol. Chem.* 272:18508–18512.

Jones, L.P., P.G. Patil, T.P. Snutch, and D.T. Yue. 1997*a*. G-protein modulation of N-type calcium channel gating current in human embryonic kidney cells (HEK 293). *J. Physiol. (Camb.).* 498:601–610.

Jones, L.P., P.G. Patil, J.G. Mulle, M.B. Sachs, and D.T. Yue. 1997*b*. Inactivation of recombinant N-type calcium channels probed by gating current analysis. *Soc. Neurosci. Abstr.* 23:475.4.

Josephson, I.R., and G. Varadi. 1996. The beta subunit increases Ca^{2+} currents and gating charge movements of human cardiac L-type Ca^{2+} channels. *Biophys. J.* 70:1285–1293.

Kamp, T.J., M.T. Perez-Garcia, and E. Marban. 1996. Enhancement of ionic current and charge movement by coexpression of calcium channel beta 1A subunit with alpha 1C subunit in a human embryonic kidney cell line. *J. Physiol. (Camb.).* 492:89–96.

Mikami, A., K. Imoto, T. Tanabe, T. Niidome, Y. Mori, H. Takeshima, S. Narumiya, and S. Numa. 1989. Primary structure and functional expression of the cardiac dihydropyridine-sensitive calcium channel. *Nature.* 340:230–233.

Mori, Y., T. Friedrich, M.S. Kim, A. Mikami, J. Nakai, P. Ruth, E. Bosse, F. Hofmann, V. Flockerzi, T. Furuichi, et al. 1991. Primary structure and functional expression from complementary DNA of a brain calcium channel. *Nature.* 350:398–402.

Neely, A., X. Wei, R. Olcese, L. Birnbaumer, and E. Stefani. 1993. Potentiation by the beta subunit of the ratio of the ionic current to the charge movement in the cardiac calcium channel. *Science.* 262:575–578.

Neher, E. 1992. Correction for liquid junction potentials in patch clamp experiments. *Methods Enzymol.* 207:123–130.

Noceti, F., P. Baldelli, X. Wei, N. Qin, L. Toro, L. Birnbaumer, and E. Stefani. 1996. Effective gating charges per channel in voltage-dependent K^+ and Ca^{2+} channels. *J. Gen. Physiol.* 108:143–155.

Olcese, R., A. Neely, N. Qin, X.Y. Wei, L. Birnbaumer, and E. Ste-

fani. 1996. Coupling between charge movement and pore opening in vertebrate neuronal alpha(1E) calcium channels. *J. Physiol. (Camb.).* 497:675–686.

Olcese, R., N. Qin, T. Schneider, A. Neely, X. Wei, E. Stefani, and L. Birnbaumer. 1994. The amino terminus of a calcium channel beta subunit sets rates of channel inactivation independently of the subunit's effect on activation. *Neuron.* 13:1433–1438.

Patil, P.G., D.L. Brody, and D.T. Yue. 1998. Preferential closed-state inactivation of neuronal calcium channels. *Neuron.* 20:1027–1038.

Perez-Reyes, E., A. Castellano, H.S. Kim, P. Bertrand, E. Baggstrom, A.E. Lacerda, X.Y. Wei, and L. Birnbaumer. 1992. Cloning and expression of a cardiac/brain beta subunit of the L-type calcium channel. *J. Biol. Chem.* 267:1792–1797.

Perez-Reyes, E., and T. Schneider. 1994. Research overview: calcium channels: structure, function and classification. *Drug Dev. Res.* 33:295–318.

Pragnell, M., M. De Waard, Y. Mori, T. Tanabe, T.P. Snutch, and K.P. Campbell. 1994. Calcium channel beta-subunit binds to a conserved motif in the I-II cytoplasmic linker of the alpha 1-subunit. *Nature.* 368:67–70.

Pragnell, M., J. Sakamoto, S.D. Jay, and K.P. Campbell. 1991. Cloning and tissue-specific expression of the brain calcium channel beta-subunit. *FEBS Lett.* 291:253–258.

Ren, D.J., and L.M. Hall. 1997. Functional expression and characterization of skeletal muscle dihypropyridine receptors in *Xenopus* oocytes. *J. Biol. Chem.* 272:22393–22396.

Schoppa, N.E., K. McCormack, M.A. Tanouye, and F.J. Sigworth. 1992. The size of gating charge in wild-type and mutant *Shaker* potassium channels. *Science.* 255:1712–1715.

Scott, V.E., M. De Waard, H. Liu, C.A. Gurnett, D.P. Venzke, V.A. Lennon, and K.P. Campbell. 1996. Beta subunit heterogeneity in N-type Ca^{2+} channels. *J. Biol. Chem.* 271:3207–3212.

Shistik, E., T. Ivanina, T. Puri, M. Hosey, and N. Dascal. 1995. Ca^{2+} current enhancement by alpha 2/delta and beta subunits in *Xenopus* oocytes: contribution of changes in channel gating and alpha 1 protein level. *J. Physiol. (Camb.).* 489:55–62.

Sigworth, F.J. 1994. Voltage gating of ion channels. *Q. Rev. Biophys.* 27:1–40.

Singer, D., M. Biel, I. Lotan, V. Flockerzi, F. Hofmann, and N. Dascal. 1991. The roles of the subunits in the function of the calcium channel. *Science.* 253:1553–1557.

Soldatov, N.M., R.D. Zuhlke, A. Bouron, and H. Reuter. 1997. Molecular structures involved in L-type calcium channel inactivation. Role of the carboxyl-terminal region encoded by exons 40-42 in alpha1S subunit in the kinetics and Ca^{2+} dependence of inactivation. *J. Biol. Chem.* 272:3560–3566.

Soong, T.W., A. Stea, C.D. Hodson, S.J. Dubel, S.R. Vincent, and T.P. Snutch. 1993. Structure and functional expression of a member of the low voltage-activated calcium channel family. *Science.* 260:1133–1136.

Stea, A., W.J. Tomlinson, T.W. Soong, E. Bourinet, S.J. Dubel, S.R. Vincent, and T.P. Snutch. 1994. Localization and functional properties of a rat brain alpha 1A calcium channel reflect similarities to neuronal Q- and P-type channels. *Proc. Natl. Acad. Sci. USA.* 91:10576–10580.

Stephens, G.J., K.M. Page, J.R. Burley, N.S. Berrow, and A.C. Dolphin. 1997. Functional expression of rat brain cloned alpha-1e calcium channels in COS7 cells. *Pflügers Arch. Eur. J. Physiol.* 433: 523–532.

Sun, D., F. Chang, A. Chien, X.-L. Xhao, R. Shirokov, E. Rios, and M. Hosey. 1994. Expression of functional cardiac L-type Ca^{2+} channels in transiently transfected HEK (293) cells. *Biophys. J.* 66: *A*320. (Abstr.)

Tareilus, E., M. Roux, N. Qin, R. Olcese, J.M. Zhou, E. Stefani, and L. Birnbaumer. 1997. A *Xenopus* oocyte beta subunit—evidence for a role in the assembly/expression of voltage-gated calcium channels that is separate from its role as a regulatory subunit. *Proc. Natl. Acad. Sci. USA.* 94:1703–1708.

Tomlinson, W.J., A. Stea, E. Bourinet, P. Charnet, J. Nargeot, and T.P. Snutch. 1993. Functional properties of a neuronal class C L-type calcium channel. *Neuropharmacology.* 32:1117–1126.

Wakamori, M., T. Niidome, D. Furutama, T. Furuichi, K. Mikoshiba, Y. Fujita, I. Tanaka, K. Katayama, A. Yatani, A. Schwartz, et al. 1994. Distinctive functional properties of the neuronal BII (class E) calcium channel. *Receptors Channels.* 2:303–314.

Walker, D., D. Bichet, K.P. Campbell, and M. De Waard. 1998. A β_4 isoform-specific interaction site in the carboxyl-terminal region of the voltage-dependent Ca^{2+} channel α_{1A} subunit. *J. Biol. Chem.* 273:2361–2367.

Walker, D., and M. De Waard. 1998. Subunit interaction in voltage-dependent Ca^{2+} channels: role in channel function. *Trends Neurosci.* 21:148–154.

Wei, X., S. Pan, W. Lang, H. Kim, T. Schneider, E. Perez-Reyes, and L. Birnbaumer. 1995. Molecular determinants of cardiac Ca^{2+} channel pharmacology. Subunit requirement for the high affinity and allosteric regulation of dihydropyridine binding. *J. Biol. Chem.* 270:27106–27111.

Wei, X.Y., E. Perez-Reyes, A.E. Lacerda, G. Schuster, A.M. Brown, and L. Birnbaumer. 1991. Heterologous regulation of the cardiac Ca^{2+} channel alpha 1 subunit by skeletal muscle beta and gamma subunits. Implications for the structure of cardiac L-type Ca^{2+} channels. *J. Biol. Chem.* 266:21943–21947.

Welling, A., E. Bosse, A. Cavalie, R. Bottlender, A. Ludwig, W. Nastainczyk, V. Flockerzi, and F. Hofmann. 1993. Stable co-expression of calcium channel alpha 1, beta and alpha 2/delta subunits in a somatic cell line. *J. Physiol. (Camb.).* 471:749–765.

Williams, M.E., P.F. Brust, D.H. Feldman, S. Patthi, S. Simerson, A. Maroufi, A.F. McCue, G. Velicelebi, S.B. Ellis, and M.M. Harpold. 1992*a*. Structure and functional expression of an omega-conotoxin-sensitive human N-type calcium channel. *Science.* 257:389–395.

Williams, M.E., D.H. Feldman, A.F. McCue, R. Brenner, G. Velicelebi, S.B. Ellis, and M.M. Harpold. 1992*b*. Structure and functional expression of alpha 1, alpha 2, and beta subunits of a novel human neuronal calcium channel subtype. *Neuron.* 8:71–84.

Williams, M.E., L.M. Marubio, C.R. Deal, M. Hans, P.F. Brust, L.H. Philipson, R.J. Miller, E.C. Johnson, M.M. Harpold, and S.B. Ellis. 1994. Structure and functional characterization of neuronal alpha 1E calcium channel subtypes. *J. Biol. Chem.* 269:22347–22357.

Witcher, D.R., M. De Waard, J. Sakamoto, C. Franzini-Armstrong, M. Pragnell, S.D. Kahl, and K.P. Campbell. 1993. Subunit identification and reconstitution of the N-type Ca^{2+} channel complex purified from brain. *Science.* 261:486–489.

Wu, L.G., J.G. Borst, and B. Sakmann. 1998. R-type Ca^{2+} currents evoke transmitter release at a rat central synapse. *Proc. Natl. Acad. Sci. USA.* 95:4720–4725.

Zagotta, W.N., and R.W. Aldrich. 1990. Voltage-dependent gating of *Shaker* A-type potassium channels in *Drosophila* muscle. *J. Gen. Physiol.* 95:29–60.